

Collective excitations in magnetic topological insulators and axion dark matter search

Koji Ishiwata^a Kentaro Nomura^b

^a*Institute for Theoretical Physics, Kanazawa University, Kanazawa 920-1192, Japan*

^b*Department of Physics, Kyushu University, Fukuoka 819-0395, Japan*

E-mail: ishiwata@hep.s.kanazawa-u.ac.jp,
nomura.kentaro@phys.kyushu-u.ac.jp

ABSTRACT: We investigate collective excitations in magnetic topological insulators (TIs) and their impact on axion detection. In the three-dimensional TI model with the Hubbard term, the effective action of magnons and amplitude modes is formulated by dynamical susceptibility under the antiferromagnetic and ferromagnetic states. One of the amplitude modes is identified as “axionic” quasi-particle and its effective coupling to the electromagnetic fields turns out to be enhanced by about four orders of magnitude larger than the previous estimate, which may drastically change the sensitivity of the axion search using “axion” in magnetic TIs.

Contents

1	Introduction	1
2	The model	3
3	Magnetic orders	4
3.1	The effective potential	4
3.2	Numerical results	7
4	The amplitude mode and magnon under magnetic order	8
4.1	Dynamical susceptibility and inverse propagator	8
4.2	The amplitude mode	9
4.3	The magnon	13
5	Implication to axion search	18
6	Conclusion	22
A	Notation	24
A.1	Gamma matrices	24
A.2	Wavefunction and Green's function	25
B	Dynamical susceptibility	26
C	Dynamical susceptibility under AFM at zero temperature	26
D	How to derive the effective action of the excitation at zero temperature	27
E	Symmetry of the Hamiltonian	29
F	Additional figures	30

1 Introduction

Axion and axion-like particles are candidates for dark matter of the universe [1–3]. While many observations have been dedicated to the search, it is yet to be found so far. Recently, the dynamical ‘axion’, as a quasi-particle in condensed matter, has drawn attention in the context of the axion dark matter search. The ‘axion’ couples to the electromagnetic field and Ref. [4] proposed an axion search in the mass range of meV using the magnetic topological insulators (TIs).¹

¹See, for examples, Refs. [5–8], for recent reviews of magnetic TIs.

The mass scale is based on an estimation of the mass of the dynamical ‘axion’ in the TIs [9]. Bi_2Se_3 , Bi_2Te_3 , and Sb_2Se_3 are the representative examples of three-dimensional (3D) TIs. Since the TIs do not have magnetic order, it is assumed in this estimation that magnetic impurities, such as Fe or Cr, are doped to Bi_2Se_3 so that the materials have ferromagnetism (FM) or antiferromagnetism (AFM). Then Ref. [9] proposes that the magnetism is described by introducing the Hubbard interaction term. Namely, the total model consists of the effective Hamiltonian for the 3D TIs and the Hubbard term. In the literature the ‘axion’ mass is estimated to be about 1 meV. On the other hand, it was shown in Ref. [10] that the typical mass of the ‘axion’ is of the order of eV, independent of the topology of insulators, in the same model. The study also indicates that it can be suppressed near the phase boundary of the AFM order. Similar results are reported in a different model in which the spin interaction term between the magnetic impurity and electron is introduced [11]. In the study the phase transitions of the AFM and FM are shown and the ‘axion’ mass is typically eV in both phases.

Determination of the ‘axion’ mass is crucial for the proposed axion search. Furthermore, it is important to find a magnetic environment that is suitable for the axion detection. In fact, the first-principles calculation shows that $\text{Mn}_2\text{Bi}_2\text{Te}_5$, which is recently synthesized experimentally [12], has a variety of magnetic states [13]. In the literature the topological phases are tuned by layer magnetization and the energy gap is computed in each magnetic state. Tuning of magnetism by an electric field in magnetically doped TIs is discussed in Ref. [14]. On the other hand, Ref. [15] claims that magnetic field induces an effective phonon charge, which plays a role of ‘axion.’ These studies inspire us to search for other possible magnetic excitations that may be utilized for the axion search.

In this paper, we investigate possible collective excitations in the magnetic TI model and study their impact on the axion detection. To this end, we revisit the original model of the magnetic TIs, i.e., the effective model for 3D TIs augmented by the Hubbard term. Starting from the partition function, the effective action for the excitations is derived using the dynamical susceptibility. The emergence of the AFM and FM orders is shown and we analyze the gap and dispersion relation of eight magnetic excitations that consist of the amplitude modes and magnons with various types.² We identify one of the amplitude modes as ‘axion’ and one of the magnons also can play the role of ‘axion’ in a specific case. The validity of the effective description of the excitations is clarified and some excitations are found to be unstable.

The paper is organized as follows. The effective action is derived from the model in Sec. 2. From the effective action the effective potential for the order parameters of the AFM and FM is calculated in Sec. 3, and the features of the magnetic orders are discussed. In Sec. 4 the effective actions of the eight types of collective excitations are derived and the dispersion relation and the stability of the excitations are described. Here we identify the ‘axion’ quasi-particle and investigate its properties. Based on the results, we discuss a direction to realistic axion search in Sec. 5. Sec. 6 is devoted to conclusion.

²The amplitude mode is also called ‘Higgs amplitude mode’ and various experimental efforts have been made to detect it, for instance, in low-dimensional magnetic materials [16–21] or frustrated magnetic materials [22, 23]. For the theory of the spin wave, see, for example, Refs. [24–28].

In our study, we adopt natural units where $\hbar = c = k_B = 1$.

2 The model

To discuss possible magnetic orders, we consider an effective Hamiltonian for 3D TIs [9, 29, 30] that is augmented by the Hubbard term. The Hamiltonian of the model is given by

$$H = H^{\text{TI}} + H_U, \quad (2.1)$$

where

$$H^{\text{TI}} = \sum_i c_i^\dagger \mathcal{H}^{\text{TI}} c_i, \quad (2.2)$$

$$H_U = U \sum_{I=A,B} \sum_i n_{Ii\uparrow} n_{Ii\downarrow}. \quad (2.3)$$

Here U is a positive constant, $I = A, B$ and i are the indices of the sublattice and site, respectively. $n_{Ii\sigma} = c_{Ii\sigma}^\dagger c_{Ii\sigma}$ is the number density of the electrons at the site with spin $\sigma = \uparrow, \downarrow$ and $c_i = (c_{Ai\uparrow}, c_{Ai\downarrow}, c_{Bi\uparrow}, c_{Bi\downarrow})^T$. \mathcal{H}^{TI} will be given later. In our study, we consider z axis as the easy axis. By the Stratonovich-Hubbard transformation, the Hubbard term is written by introducing two fields ϕ_{Ii} :

$$H_U \rightarrow \frac{U}{4} \sum_{I,i} [\phi_{Ii}^2 + 2\phi_{Ii}(n_{Ii\uparrow} - n_{Ii\downarrow})] \quad (2.4)$$

$$= \frac{U}{2} \sum_i (\phi_{fi}^2 + \phi_{ai}^2) + \frac{U}{2} \sum_i c_i^\dagger [\phi_{ai}\Gamma^5 + \phi_{fi}\Gamma^{12}] c_i, \quad (2.5)$$

where Γ^{12} and Γ^5 are 4 by 4 matrices defined as

$$\Gamma^5 = \begin{pmatrix} \sigma^3 & 0 \\ 0 & -\sigma^3 \end{pmatrix}, \quad \Gamma^{12} = \begin{pmatrix} \sigma^3 & 0 \\ 0 & \sigma^3 \end{pmatrix}. \quad (2.6)$$

Here $\vec{\sigma} = (\sigma^1, \sigma^2, \sigma^3)$ are the Pauli matrices. Appendix A.1 gives the list of the Gamma matrices that are used in this study. ϕ_{Ii} is physically the spin moment in z direction at site i of sublattice I and we have introduced

$$\phi_{ai} \equiv (\phi_{Ai} - \phi_{Bi})/2, \quad (2.7)$$

$$\phi_{fi} \equiv (\phi_{Ai} + \phi_{Bi})/2. \quad (2.8)$$

When ϕ_{ai} and ϕ_{fi} are constants, then their constant values correspond to the order parameters of the AFM and FM, respectively. The term proportional to Γ^{12} is considered in Refs. [31–33] in different models. Then (Euclidean) action is given by

$$S = \int_0^\beta d\tau \sum_i \left[c_i^\dagger (\partial_\tau + \mathcal{H}) c_i + \frac{U}{2} (\phi_{ai}^2 + \phi_{fi}^2) \right] \quad (2.9)$$

where $\tau = it$ is the imaginary time and

$$\mathcal{H} = \mathcal{H}^{\text{TI}} + (U/2)(\phi_{ai}\Gamma^5 + \phi_{fi}\Gamma^{12}). \quad (2.10)$$

$\beta = T^{-1}$ is the inverse temperature. The effective action S_{eff} is given by integrating out the electron field c_i in the partition function Z , i.e.,

$$\begin{aligned} Z &= \int \mathcal{D}c \mathcal{D}c^\dagger \mathcal{D}\phi_a \mathcal{D}\phi_f e^{-S} \\ &= \int \mathcal{D}\phi_a \mathcal{D}\phi_f e^{-S_{\text{eff}}}, \end{aligned} \quad (2.11)$$

which leads to

$$S_{\text{eff}} = \int_0^\beta d\tau \frac{U}{2} \sum_i (\phi_{ai}^2 + \phi_{fi}^2) - \ln \det(\partial_\tau + \mathcal{H}). \quad (2.12)$$

We will use Z and S_{eff} to derive the effective potential for the order parameters in the next section.

3 Magnetic orders

In this section we find possible global orders of the magnetism and identify the ground state. For this purpose, we ignore the local quantum fluctuations and compute the effective potential following the technique of Ref. [11].

3.1 The effective potential

The effective potential is derived from the grand potential. The grand potential Ω is defined by the partition function Z :³

$$\Omega = -\beta^{-1} \ln Z. \quad (3.1)$$

The effective potential per site is then obtained by taking ϕ_{ai} and ϕ_{fi} as constants, i.e., $\phi_{ai} = \phi_a$ and $\phi_{fi} = \phi_f$,

$$\begin{aligned} V_{\text{eff}} &\equiv -\beta^{-1} \ln e^{-S_{\text{eff}}}/N|_{(\phi_{ai}, \phi_{fi})=(\phi_a, \phi_f)} \\ &= \frac{U}{2}(\phi_f^2 + \phi_a^2) - \frac{1}{\beta N} \sum_{h, \mathbf{k}} \ln(1 + e^{-\beta(E_{h\mathbf{k}} - \mu)}), \end{aligned} \quad (3.2)$$

where N is the number of the cite, μ is the chemical potential, h is the band index, and \mathbf{k} is the wavenumber. $E_{h\mathbf{k}}$ will be given soon. In the derivation, we have adopted the Matsubara formalism, which gives

$$\ln \det(\partial_\tau + \mathcal{H}) = \sum_n \sum_{h, \mathbf{k}} \ln(-i\omega_n + E_{h\mathbf{k}} - \mu), \quad (3.3)$$

³Though we give the formulae with finite temperature, we will focus on the zero temperature limit in the later numerical study.

where $\omega_n = (2n + 1)\pi/\beta$ is the Matsubara frequency for fermion. $E_{h\mathbf{k}}$ are the eigenvalues of $\mathcal{H}_{\mathbf{k}}$, which is \mathcal{H} in the wavenumber space:

$$\mathcal{H}_{\mathbf{k}} = \mathcal{H}_{\mathbf{k}}^{\text{TI}} + d_5 \Gamma^5 + d_{12} \Gamma^{12}, \quad (3.4)$$

where

$$\mathcal{H}_{\mathbf{k}}^{\text{TI}} = \epsilon_0 \mathbf{1} + \sum_{a=1}^4 d_a \Gamma^a, \quad (3.5)$$

$$(d_5, d_{12}) = (U/2)(\phi_a, \phi_f). \quad (3.6)$$

Γ^a ($a = 1-4$) are the Gamma matrices given by

$$\Gamma^1 = \begin{pmatrix} \sigma^1 & 0 \\ 0 & -\sigma^1 \end{pmatrix}, \quad \Gamma^2 = \begin{pmatrix} \sigma^2 & 0 \\ 0 & -\sigma^2 \end{pmatrix}, \quad \Gamma^3 = \begin{pmatrix} 0 & -i\mathbf{1} \\ i\mathbf{1} & 0 \end{pmatrix}, \quad \Gamma^4 = \begin{pmatrix} 0 & -\mathbf{1} \\ -\mathbf{1} & 0 \end{pmatrix}, \quad (3.7)$$

and we take $\phi_a, \phi_f > 0$ without loss of generality. ϵ_0 is a constant and d^a is parametrized as [9, 29, 30]

$$(d_1, d_2, d_3, d_4) = (A_2 \sin k_x a_x, A_2 \sin k_y a_y, A_1 \sin k_z a_z, \mathcal{M}), \quad (3.8)$$

where $\mathcal{M} = M_0 - 2B_1 - 4B_2 + 2B_1 \cos k_z a_z + 2B_2(\cos k_x a_x + \cos k_y a_y)$. In the following study, we consider a cubic lattice and use dimensionless wavenumber for simplicity, i.e., $a_x = a_y = a_z = 1$. The first and second terms of $\mathcal{H}_{\mathbf{k}}$ have the time-reversal invariance, which is one of the features of the TIs, and it describes Bi_2Se_3 family of materials. The eigenvalues are obtained as $(E_{1\mathbf{k}}, E_{2\mathbf{k}}, E_{3\mathbf{k}}, E_{4\mathbf{k}}) = (\epsilon_0 - \epsilon_{1\mathbf{k}}, \epsilon_0 - \epsilon_{2\mathbf{k}}, \epsilon_0 + \epsilon_{1\mathbf{k}}, \epsilon_0 + \epsilon_{2\mathbf{k}})$, where

$$\epsilon_{1\mathbf{k}} = \sqrt{d_0^2 - d_s^2 + [d_{12} + (d_s^2 + d_5^2)^{1/2}]^2}, \quad (3.9)$$

$$\epsilon_{2\mathbf{k}} = \sqrt{d_0^2 - d_s^2 + [d_{12} - (d_s^2 + d_5^2)^{1/2}]^2}, \quad (3.10)$$

Here $d_0 \equiv (\sum_{a=1}^4 d_a^2)^{1/2}$ and $d_s \equiv (d_3^2 + d_4^2)^{1/2}$. Since we focus on the insulated states, we consider that the electrons are half-filled. Namely, we take $\epsilon_0 - \mu \simeq 0$ and two lower bands $E_{1\mathbf{k}}$ and $E_{2\mathbf{k}}$ are filled.

For later analysis, we derive the stationary conditions for the possible magnetic orders. For the AFM, it is given by $\partial V_{\text{eff}}/\partial \phi_a|_{(\phi_a, \phi_f)=(\phi_{a0}, 0)} = 0$, and the result is

$$1 + \frac{U}{2N} \sum_{\mathbf{k}} \{-n_F(-d) + n_F(d)\} \frac{1}{d} = 0, \quad (3.11)$$

where ϕ_{a0} is a nonzero stationary value, $d \equiv (\sum_{a=1}^5 d_a^2)^{1/2}$ and n_F is the Fermi-Dirac distribution function. Similarly, $\partial V_{\text{eff}}/\partial \phi_f|_{(\phi_a, \phi_f)=(0, \phi_{f0})} = 0$ gives a nonzero ϕ_{f0} that satisfies

$$1 + \frac{1}{2N\phi_{f0}} \sum_{\mathbf{k}} \left[\{-n_F(-\epsilon_1) + n_F(\epsilon_1)\} \frac{d_{12} + d_s}{\epsilon_1} + \{-n_F(-\epsilon_2) + n_F(\epsilon_2)\} \frac{d_{12} - d_s}{\epsilon_2} \right] = 0. \quad (3.12)$$

For both the AFM and FM cases, it is easy to check that $\phi_{a0}, \phi_{f0} \rightarrow 1$ as $U \rightarrow \infty$, which corresponds to a case where the magnetism is saturated.

Before computing the effective potential, we discuss conditions for the AFM and FM orders. To this end we take $T \rightarrow 0$ limit, which leads to

$$V_{\text{eff}}|_{T=0} = \frac{U}{2}(\phi_f^2 + \phi_a^2) - \frac{1}{N} \sum_{\mathbf{k}} (\epsilon_{1\mathbf{k}} + \epsilon_{2\mathbf{k}}). \quad (3.13)$$

Regarding the AFM, we expand the effective potential up to $\mathcal{O}(\phi_a^2)$ while taking $\phi_f = 0$ to obtain

$$V_{\text{eff}}|_{T=0, \phi_f=0} = \frac{U}{2} \phi_a^2 \left[1 - \frac{U}{2N} \sum_{\mathbf{k}} \frac{1}{d_0} \right] + \mathcal{O}(\phi_a^4) + \text{const.} \quad (3.14)$$

Therefore we expect to have the AFM order when

$$1 - \frac{U}{2N} \sum_{\mathbf{k}} \frac{1}{d_0} < 0. \quad (3.15)$$

Similarly, one may get a condition to have the FM order as

$$1 - \frac{U}{2N} \sum_{\mathbf{k}} \frac{d_1^2 + d_2^2}{d_0^3} < 0. \quad (3.16)$$

However, it is not an exact condition for the FM order; the FM order may arise even when (3.16) is not satisfied. This can be understood by expanding the effective potential at $\mathcal{O}(\phi_f^4)$:

$$V_{\text{eff}}|_{T=0, \phi_a=0} = \frac{U}{2} \phi_f^2 \left[1 - \frac{U}{2N} \sum_{\mathbf{k}} \frac{d_1^2 + d_2^2}{d_0^3} \right] + \frac{U^4 \phi_f^4}{64} \sum_{\mathbf{k}} \frac{d_0^4 - 6d_0^2 d_s^2 + 5d_s^4}{d_0^7} + \mathcal{O}(\phi_f^6). \quad (3.17)$$

The coefficient of a term proportional to ϕ_f^4 can be negative, which may lead to the FM order. We will confirm this numerically later. Even though it is not an exact condition, (3.16) can be used to understand the qualitative behavior of the emergence of the magnetic order. I.e., we expect that the FM order will appear for relatively larger d_1 and d_2 than d_3 and d_4 , in other words, larger A_2 compared to A_1 , B_1 , B_2 , and M_0 .

On the other hand, if $d_1 = d_2 = 0$ is exactly satisfied, the effective potential becomes

$$V_{\text{eff}}|_{T=0, \phi_a=0} = \frac{U}{2} \phi_f (\phi_f - 2). \quad (3.18)$$

Thus, the FM order appears without other conditions, and the stationary point is given by $\phi_{f0} = 1$. We will discuss this specific case later.

Both conditions (3.15) and (3.16) are satisfied in the limit $U \rightarrow \infty$. Thus, the AFM and FM order should appear in the large U limit.

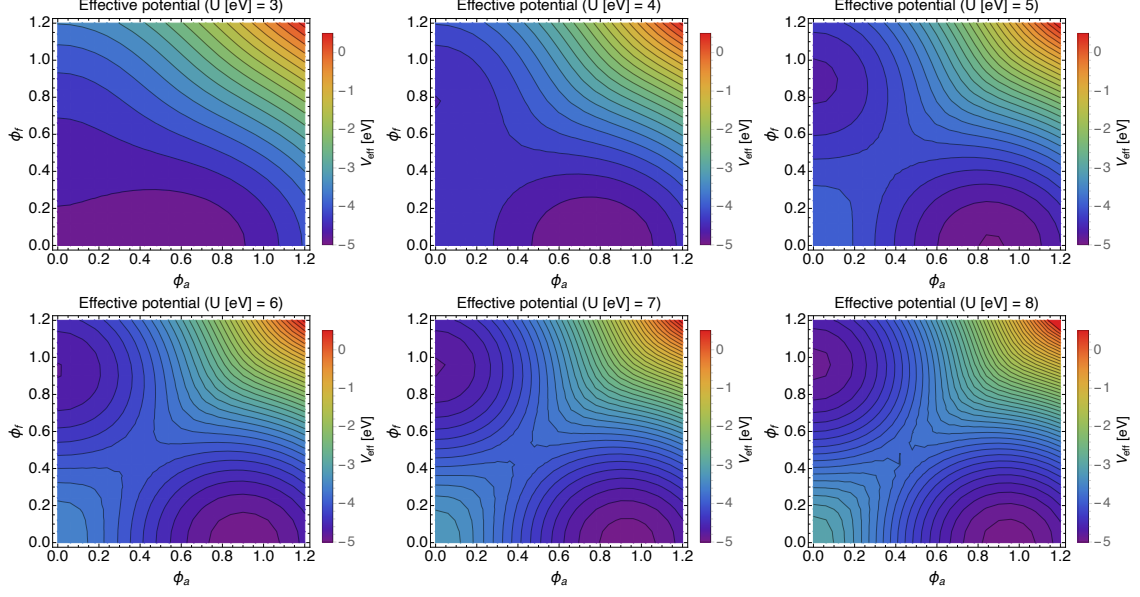


Figure 1. Effective potential on (ϕ_a, ϕ_f) plane at $T = 0$. Each panel corresponds to different values of U . The other parameters are $A_1 = A_2 = 1$ eV, $B_1 = B_2 = -0.05$ eV, and $M_0 = 0.01$ eV. Their definitions are given in Eq. (3.8) and the below.

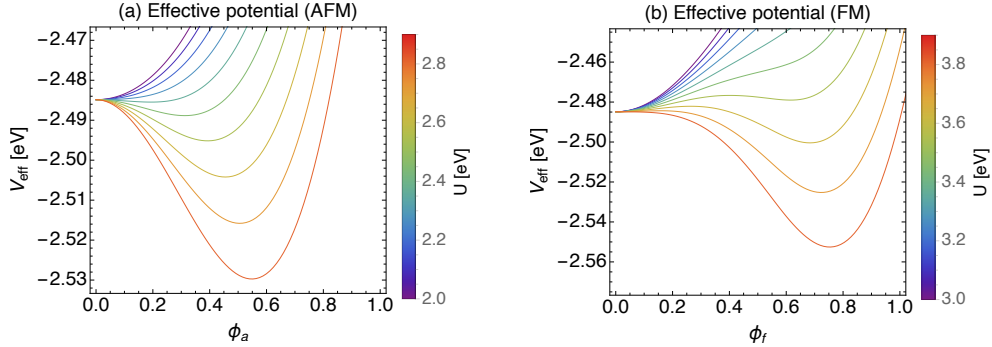


Figure 2. (a) Effective potential under $\phi_f = 0$ as function of ϕ_a with various values of U indicated in the color bar. (b) The same as (a) but under $\phi_a = 0$ as function of ϕ_f . For both panels, the parameters A_1, A_2, B_1, B_2 , and M_0 are the same as Fig. 1.

3.2 Numerical results

Now we are ready to show the effective potential on (ϕ_a, ϕ_f) plane. Fig. 1 shows the effective potential for a given set of parameters. We take $T = 0$ and the normal insulator (NI) phase is considered. The TI phase can be calculated by taking $M_0 < 0$ with the others being unchanged and we found the result merely changes. It is seen the potential minima appear as U increases. As U gets large, the AFM order forms first since the condition for the AFM order, i.e., (3.15), is relatively easy to satisfy, and eventually the FM order shows up.

To see the emergence of the magnetic orders, Fig. 2 shows the effective potential as

function ϕ_a or ϕ_f . It should be noted that ϕ_{a0} appears continuously from zero meanwhile the non-zero ϕ_{f0} is obtained discontinuously. For the FM order, it is seen that another vacuum appears as the U becomes larger while the coefficient of the quadratic term is positive. This is due to the negative ϕ_f^4 term in Eq. (3.17). Such a situation never happens for the AFM since the quartic term is always positive. In fact, the phase transition to the AFM order happens when the value of U exceeds a critical value U_c^{AFM} defined by

$$U_c^{\text{AFM}} = \left(\frac{1}{2N} \sum_{\mathbf{k}} \frac{1}{d_0} \right)^{-1}. \quad (3.19)$$

In the present parameter set, i.e., $A_1 = A_2 = 1$ eV, $B_1 = B_2 = -0.05$ eV, and $M_0 = 0.01$ eV, we find $U_c^{\text{AFM}} \sim 2$ eV.

Regarding to the ground state of the magnetic order, we have numerically checked that the minimum of the effective potential is obtained when the magnetic state is the AFM. This is true for other sets of parameters. Therefore, the ground state of the system is the AFM order. On the other hand, both minima for the AFM and FM orders get degenerate as $U \rightarrow \infty$. This can be understood analytically. In the large U limit, the stationary points (ϕ_{a0}, ϕ_{f0}) reduce to $(1, 0)$ and $(0, 1)$ and $\epsilon_{1\mathbf{k}}, \epsilon_{2\mathbf{k}} \simeq U/2$. Thus both minima approach to

$$V_{\text{eff}}|_{T=0} \rightarrow \frac{U}{2} - \frac{1}{N} \sum_{\mathbf{k}} 2 \times \frac{U}{2} = -\frac{U}{2}. \quad (3.20)$$

Therefore, when the magnetization is saturated, i.e., $\phi_{a0}, \phi_{f0} \simeq 1$, both AFM and FM orders are expected to be realized as quasi-degenerate vacua.

To summarize, we have seen the emergence of the AFM and FM orders by computing the effective potential from the grand potential and found that the AFM is the ground state. On the other hand, the AFM and FM states are degenerate as U gets larger.

4 The amplitude mode and magnon under magnetic order

In this section, we evaluate the gap and dispersion relation of the magnetic excitations under the magnetic orders. As seen in the previous section, the possible magnetic orders are the AFM and FM and the former is the ground state. To consider the excitations under both magnetic environments, we take $(\phi_{ai}, \phi_{fi}) = (\phi_{a0}, 0)$ or $(0, \phi_{f0})$, where ϕ_{a0} and ϕ_{f0} are constants that satisfy Eqs. (3.11) and (3.12), respectively. We will see that there are two magnetic excitations, that are amplitude mode and magnon, and each of them has two types. Fig. 3 (left panel) shows the classification of the excitations. We will also discuss an excitation called ‘axion’ in the magnetic TIs.

4.1 Dynamical susceptibility and inverse propagator

For the study we introduce a dynamical susceptibility, which is defined by

$$\chi_M(k; O_1, O_2) = -\frac{1}{\beta N} \sum_{i\omega_\ell, \ell} \text{Tr}[\tilde{G}_M(\ell) O_1 \tilde{G}_M(\ell + k) O_2], \quad (4.1)$$

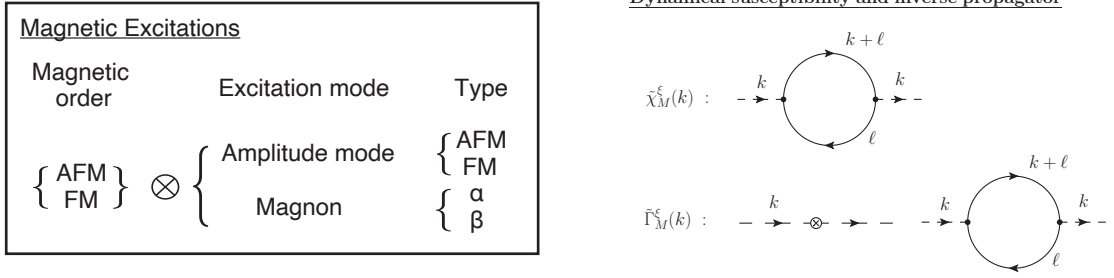


Figure 3. (Left) Classification of the magnetic excitations. Excitation modes are amplitude mode and magnon. The amplitude mode has ‘AFM-type’ and ‘FM-type,’ defined in Eqs. (4.4) and (4.5), and the magnon has ‘ α -type’ and ‘ β -type,’ defined in Eqs. (4.27) and (4.28). Images of the amplitude mode and magnons are shown in Figs. 4 and 6, respectively. (Right) Diagram corresponding to dynamical susceptibility $\tilde{\chi}_M^\xi(k)$ and the (dimensionless) inverse propagator $\tilde{\Gamma}_M^\xi(k)$. $k = (i\omega_n, \mathbf{k})$ and $\ell = (i\omega_\ell, \mathbf{\ell})$ are external and loop momenta, respectively. Dashed line shows the magnetic excitations, amplitude mode or magnon, and solid line shows electron. In the definitions of $\tilde{\chi}_M^\xi$ and $\tilde{\Gamma}_M^\xi$, the external lines of the excitations are excluded. Blobs are vertices and a set of Γ^5 , Γ^{12} , Γ^\pm , or Σ^\pm enters depending on the excitations. Crossed blob stands for the tree-level vertex or tadpole.

where \tilde{G}_M is the Green’s function of the electron under the global magnetic order, AFM or FM, in the wavenumber space, which will be defined soon. The index $M = A$ and F stands for the magnetic order, i.e., AFM and FM, respectively. O_1 and O_2 are four by four matrices, such as Gamma matrices. For the arguments of the susceptibility and the Green’s function, we write k and ℓ as $k = (i\omega_n, \mathbf{k})$ and $\ell = (i\omega_\ell, \mathbf{\ell})$. Instead of χ_M , we will use a dynamical susceptibility that is symmetric with respect to O_1 and O_2 :

$$\tilde{\chi}_M^\xi(k) \equiv \frac{1}{2} \{ \chi_M(k; O_1, O_2) + \chi_M(k; O_2, O_1) \}, \quad (4.2)$$

Here ξ is a label for a specific set of operators O_1 and O_2 , which will be given explicitly in this section.

With the dynamical susceptibility, we will see that $\tilde{\Gamma}_M^\xi(k)$ defined by

$$\tilde{\Gamma}_M^\xi(k) \equiv 1 - \frac{U}{4} \tilde{\chi}_M^\xi(k), \quad (4.3)$$

plays the role of the inverse propagator, which is normalized to be dimensionless, of the excitations at the one-loop level. Fig. 3 (right panel) shows diagrams that correspond to the dynamical susceptibility $\tilde{\chi}_M^\xi$ and the inverse propagator $\tilde{\Gamma}_M^\xi$.

4.2 The amplitude mode

To discuss the amplitude mode, we take

$$\phi_{ai} = \phi_{a0} + \delta\phi_{ai}, \quad (4.4)$$

$$\phi_{fi} = \phi_{f0} + \delta\phi_{fi}. \quad (4.5)$$

$\delta\phi_{ai}$ and $\delta\phi_{fi}$ are two independent fluctuations of the AFM and FM order parameters, respectively, and we call them ‘AFM-type’ and ‘FM-type.’ The example of the fluctuations

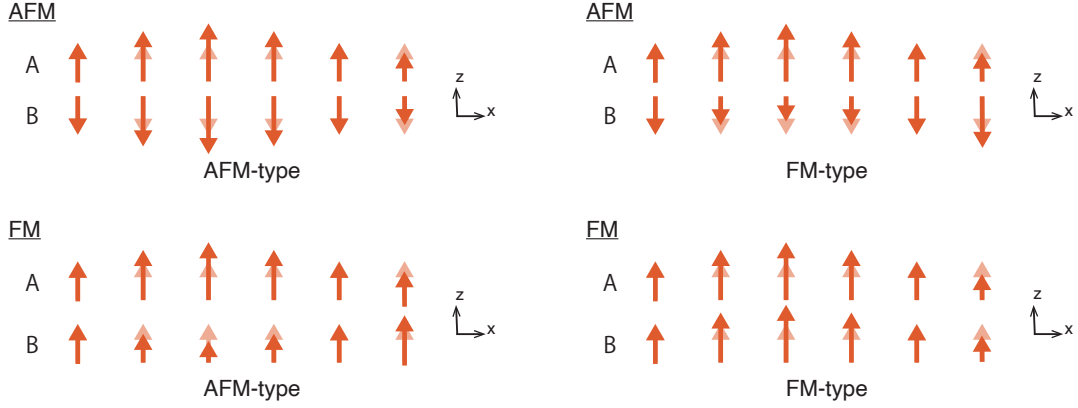


Figure 4. Image of the amplitude mode under the AFM (top) and FM (bottom) orders. The AFM-type (left) and FM-type (right) is shown. The plot is an example of the excitation with a wavenumber $\mathbf{k} = (\pi/4, 0, 0)$.

are shown in Fig. 4. One can imagine that there are four excitations by looking at the effective potential in Fig. 1; the AFM- and FM-type amplitude modes under the AFM correspond to the fluctuations around $(\phi_a, \phi_f) = (\phi_{a0}, 0)$ in ϕ_a and ϕ_f directions, respectively, and a similar interpretation applies to the fluctuations around $(\phi_a, \phi_f) = (0, \phi_{f0})$. From the figure we naively expect all the amplitude modes to be stable. This intuition, however, needs to be modified, which will be discussed below.

With Eqs. (4.4) and (4.5), we expand the second term of Eq. (2.12) as⁴

$$\begin{aligned} -\ln \det(\partial_\tau + \mathcal{H}) &= -\text{Tr} \ln(\partial_\tau + \mathcal{H}) \\ &= -\text{Tr} \ln(-G_M^{-1}) + \sum_{n=1}^{\infty} \text{Tr}(G_M \delta \mathcal{H})^n, \end{aligned} \quad (4.6)$$

by decomposing $\mathcal{H} = \mathcal{H}^{\text{MTI}} + \delta \mathcal{H}$ where

$$\mathcal{H}^{\text{MTI}} = \mathcal{H}^{\text{TI}} + (U/2)(\phi_{a0}\Gamma^5 + \phi_{f0}\Gamma^{12}), \quad (4.7)$$

$$\delta \mathcal{H} = (U/2)(\delta \phi_{ai}\Gamma^5 + \delta \phi_{fi}\Gamma^{12}). \quad (4.8)$$

Then the Green's function is given by $G_M^{-1} = -\partial_\tau - \mathcal{H}^{\text{MTI}}$ where $\phi_{f0} = 0$ and $\phi_{a0} = 0$ for $M = A$ and F , respectively. Using the definition of the Fourier expansion of the field and

⁴Similar expansion is done in Refs. [8, 34, 35] to derive ‘axion’ mass, meanwhile the first term of Eq. (2.5), i.e., $U\phi_{ai}^2/2$ that will give rise to a term $U\delta\phi_{ai}^2/2$ in Eq. (4.9), is missing at the beginning. When this term is missing, then the resultant ‘mass term’ gets the opposite sign, leading to the tachyonic instability. The authors, however, claim that they obtain the same result as one in Ref. [9] though their calculation is inconsistent. See also discussion below Eq. (4.15).

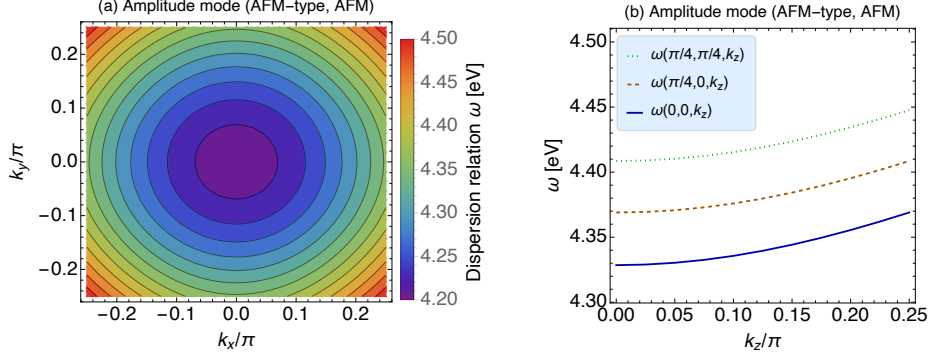


Figure 5. Dispersion relation for the AFM-type amplitude mode under the AFM. (a) Contour of $\omega(k_x, k_y, 0)$. (b) $\omega(\mathbf{k})$ as function of k_z for various values of k_x, k_y . We take $U = 5$ eV and the other parameters are the same as Fig. 1.

the Green's function given in Appendix A.2, the effective action at $\mathcal{O}(\delta\phi_{ai}^2, \delta\phi_{fi}^2)$ is

$$S_{\text{eff}} \supset \int_0^\beta d\tau \sum_i \sum_{\xi=a,f} \frac{U}{2} \delta\phi_{\xi i}^2 + \frac{1}{2} \text{Tr}(G\delta\mathcal{H})^2 \quad (4.9)$$

$$= \frac{U}{2} \sum_{i\omega_n, \mathbf{k}} \sum_{\xi=a,f} \delta\tilde{\phi}_\xi(\mathbf{k}) \delta\tilde{\phi}_\xi(-\mathbf{k}) \tilde{\Gamma}_M^\xi(\mathbf{k}), \quad (4.10)$$

where $\tilde{\Gamma}_M^\xi$ is given in Eq. (4.3) and

$$\tilde{\chi}_M^a(\mathbf{k}) = \chi_M(\mathbf{k}; \Gamma^5, \Gamma^5), \quad (4.11)$$

$$\tilde{\chi}_M^f(\mathbf{k}) = \chi_M(\mathbf{k}; \Gamma^{12}, \Gamma^{12}). \quad (4.12)$$

The first term of $\tilde{\Gamma}_M^\xi(\mathbf{k})$ comes from the first term in Eq. (4.9), which is the tree-level contribution mass term and the second one corresponds to the loop diagram. $\tilde{\Gamma}_M^\xi(\mathbf{k})$ plays a role of an inverse propagator of the excitations at the one-loop level while it is normalized to dimensionless in our notation. Thus $1/\tilde{\Gamma}_M^\xi(\mathbf{k})$ plays a role of the connected two-point Green's function that is given by summing over the infinite series of the one-loop diagram. $\tilde{\chi}_M^\xi(\mathbf{k})$ can be evaluated in the basis where the Green's functions are diagonalized. The calculation is shown in Appendix B. From Eq. (4.10), the gap and dispersion relation $\omega = \omega(\mathbf{k})$ of the amplitude mode is given by solving

$$\tilde{\Gamma}_M^\xi(i\omega_n = \omega + i\delta, \mathbf{k}) = 0, \quad (4.13)$$

where $\delta \ll 1$.

Before the numerical study, we comment on the ‘axionic’ excitation in the magnetic TIs. We claim that the AFM-type amplitude mode under the AFM order corresponds to the quasi-particle ‘axion,’ regardless of the topological nature of the insulators. Namely, the ‘axion’ corresponds to the AFM-type amplitude mode in both TI and NI phases.⁵

⁵The existence of the dynamical ‘axion’ in NIs with the AFM state is already pointed out in Ref. [36]. The dynamical ‘axion’ is also studied under the FM order in Ref. [11, 33].

First of all, the gap of the AFM-type amplitude mode under the AFM order, obtained by Eq. (4.13), corresponds to the mass of the ‘axion’. This fact is understood from the fact that $\tilde{\Gamma}_M^m$ is the inverse propagator of the excitation and that the pole of the propagator gives the physical mass. To derive the effective action for the ‘axion,’ let us take the zero temperature limit. First, the mass m_a of ‘axion’ is given by

$$\tilde{\Gamma}_A^a(i\omega_n = m_a, \mathbf{0}) = 0. \quad (4.14)$$

It is easy to find a solution for the equation by using an analytic expression for $\tilde{\chi}_A^a$ given Eq. (C.1) of Appendix C:

$$m_a = U\phi_{a0} (= 2d_5), \quad (4.15)$$

for $\phi_{a0} \neq 0$.⁶ Then, expanding $\tilde{\Gamma}_A^a$ at $i\omega_n = m_a$ and $\mathbf{k} = \mathbf{0}$ and taking a continuum limit for the space, we get the action of the ‘axion’ in the Minkowski spacetime as

$$S_a = \left(\frac{U}{2}\right)^2 J \int d^4x \delta\phi_a [-\partial_t^2 + v_i^2 \partial_i^2 - m_a^2] \delta\phi_a, \quad (4.16)$$

where an index i is summed from 1 to 3 and

$$J = \int \frac{d^3\ell}{(2\pi)^3} \frac{1}{4dd_0^2}, \quad (4.17)$$

Here J and v_i are the stiffness and velocity, respectively. See Appendix D for the derivation of the action. The results of the mass and stiffness given in Eqs. (4.15) and (4.17) are different from the previous results [10]⁷

$$J^{\text{old}} = \int \frac{d^3\ell}{(2\pi)^3} \frac{d_0^2}{4d^5}, \quad (4.18)$$

$$J^{\text{old}}(m_a^{\text{old}})^2 = \int \frac{d^3\ell}{(2\pi)^3} \frac{d_5^2}{d^3}. \quad (4.19)$$

The reason is that the previous results are given by expanding $\tilde{\Gamma}_A^a(i\omega_n, \mathbf{0})$ at $i\omega_n = 0$, not $i\omega_n = m_a$. This is based on the assumption that the expansion around $i\omega_n = 0$ is a good approximation. However, the quantitative argument regarding the validity of the expansion around $i\omega_n = 0$ has not been clarified explicitly in the previous works.

Compared to the previous calculation, we have two improvements. First, the mass and stiffness given in the present work are more accurate. This is because we do not use perturbative expansion to derive the mass and that the stiffness is derived by the derivative of $\tilde{\Gamma}_A^a$ with respect to $(i\omega_n)^2$ at the mass. Second, it is possible to check whether the gap (or mass) obtained at $\mathbf{k} = \mathbf{0}$ is the minimum. Namely, there is a possibility that a smaller gap is obtained for a nonzero \mathbf{k} . In such a case, we must expand $\tilde{\Gamma}_A^a$ at the wavenumber

⁶The ‘axion’ mass can be obtained by solving $\tilde{\Gamma}_A^a(i\omega_n = m_a, \mathbf{0}) = 0$ numerically for $\phi_{a0} = 0$ case.

⁷ J and Jm_a^2 in Refs. [8, 9, 34, 35] are smaller than those in Ref. [10] by a factor of 4, which was already pointed out in Ref. [10].

to derive the effective action for the lower-energy excitation. We will check this possibility numerically below.

By the use of the effective action, we can evaluate the validity condition of the perturbative expansion of the past works. As a result, we found that the expansion is valid for $m_a \lesssim \mathcal{O}(\text{eV})$. The details are given in Appendix D.

Fig. 5 shows the dispersion relation of the AFM-type amplitude mode under the AFM order. We take $U = 5$ and the other parameters are the same as Fig. 1. We found that $\mathbf{k} = \mathbf{0}$ is the stable minimum. Here ‘stable’ means that the curvature of the dispersion relation $\omega = \omega(\mathbf{k})$ is positive in all \mathbf{k} directions around $\mathbf{k} = \mathbf{0}$. In other word, v_i^2 are positive for all $i = 1-3$. This can be seen explicitly in the figure. We have checked that there are no smaller gaps, thus the gap is surely given by $m_a = U\phi_{a0} \sim \mathcal{O}(\text{eV})$.

The situation is different for the other amplitude modes. As an example, let us discuss the FM-type amplitude mode with the AFM order. The dynamical susceptibility of the excitation is analytically obtained by (see Appendix C)

$$\tilde{\chi}_A^f(\omega + i\delta, \mathbf{k}) = \frac{2}{N} \sum_{\ell} \frac{df - \sum_{a=1}^5 d_a f_a + 2(d_1 f_1 + d_2 f_2)}{df(d+f)} \frac{1}{1 - (\omega^2 + i\delta)/(d+f)^2}, \quad (4.20)$$

where d_a and f_a ($a = 1-4$) depend on the wavenumber as $d_a = d_a(\ell)$, $f_a = d_a(\ell + \mathbf{k})$, $f_5 = d_5$, and $f = (\sum_{a=1}^5 f_a f_a)^{1/2}$. When $\mathbf{k} = 0$, for instance, we found that the gap is found to satisfy $\omega(\mathbf{0}) > \omega_c$, where $\omega_c = \text{Min}(2d)$. In addition, the imaginary part of $\tilde{\chi}_A^f$ is enhanced. This indicates that the amplitude mode tends to dissipate to an electron-hole pair. One can understand the interpretation of the imaginary part from a corresponding diagram to the dynamical susceptibility, shown in Fig. 3. Similar behavior is found for nonzero \mathbf{k} . Therefore, the excitation is not stable and dissipates even if it is created. We have also found no stable configuration for both AFM- and FM-type amplitude modes under the FM order. In addition, the expansion for ω is inappropriate since $\omega/(d+f)$ can be larger than unity. Therefore, the effective description of the form of Eq. (4.16) is invalid for those excitations.

4.3 The magnon

To describe the magnon, we need to rewrite the Hubbard term in an isotropic form. Namely, the Stratonovich-Hubbard transformation gives

$$H_U \rightarrow \frac{U}{4} \sum_{I,i} \left[\phi_I^2 + 2\phi_I c_{Ii}^\dagger \vec{n}_{Ii} \cdot \vec{\sigma} c_{Ii} \right], \quad (4.21)$$

where $\vec{n}_{Ii} = (n_{Ii}^x, n_{Ii}^y, n_{Ii}^z)$ that satisfies $|\vec{n}_{Ii}| = 1$. Under the AFM, $\phi_{Ai} = -\phi_{Bi} = \phi_{a0}/2$, while $\phi_{Ai} = \phi_{Bi} = \phi_{f0}/2$ for the FM. Recalling that we are interested in the case where z direction is the easy axis, the fluctuation of n_{Ii}^x, n_{Ii}^y corresponds to the magnon. For later analysis we introduce $\vec{n}_{\alpha i}$ and $\vec{n}_{\beta i}$ as

$$\vec{n}_{\alpha i} \equiv (\vec{n}_{Ai} + \vec{n}_{Bi})/2, \quad (4.22)$$

$$\vec{n}_{\beta i} \equiv (\vec{n}_{Ai} - \vec{n}_{Bi})/2. \quad (4.23)$$

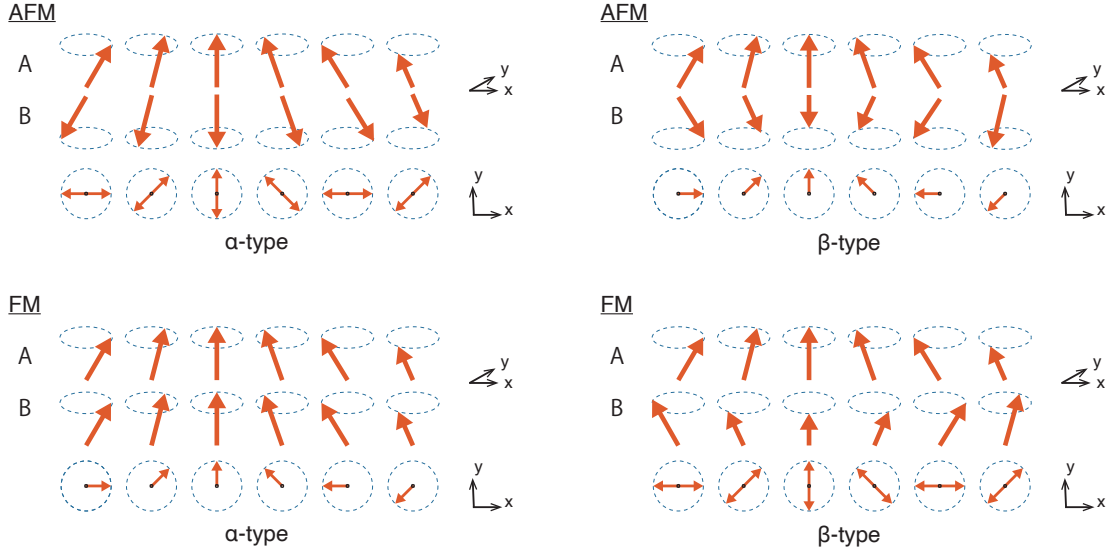


Figure 6. Image of the magnon under the AFM (top) and FM (bottom) orders. The plot is an example of the excitation with a wavenumber $\mathbf{k} = (\pi/4, 0, 0)$.

The labels α and β stand for two different types of magnon excitations, which we call ‘ α -type’ and ‘ β -type,’ respectively. We will formulate each excitation under both the AFM and FM orders below.

First, let us discuss the magnon under the AFM order. \vec{n}_A and \vec{n}_B are parallel for the α -type, meanwhile rotation phases of \vec{n}_A and \vec{n}_B coincide for the β -type. See Fig. 6 (top panel) for an example of the α - and β -types under the AFM. The interaction Hamiltonian gives

$$H_U \supset \frac{U\phi_{a0}}{2} \sum_i c_i^\dagger \left[\Gamma^5 n_{\alpha i}^z + \Gamma^1 n_{\alpha i}^x + \Gamma^2 n_{\alpha i}^y + \Gamma^{12} n_{\beta i}^z + \Gamma^{25} n_{\beta i}^x + \Gamma^{51} n_{\beta i}^y \right] c_i, \quad (4.24)$$

where

$$\Gamma^{25} = \begin{pmatrix} \sigma^1 & 0 \\ 0 & \sigma^1 \end{pmatrix}, \quad \Gamma^{51} = \begin{pmatrix} \sigma^2 & 0 \\ 0 & \sigma^2 \end{pmatrix}. \quad (4.25)$$

Assuming that $n_{\alpha i}^x, n_{\alpha i}^y, n_{\beta i}^x, n_{\beta i}^y \ll 1$ the Hamiltonian reduces to $\mathcal{H} = \mathcal{H}^{\text{MTI}} + \delta\mathcal{H}$ where

$$\delta\mathcal{H} = \frac{U\phi_{a0}}{2} \left[-\frac{1}{2} \Gamma^5 \{ (n_{\alpha i}^x)^2 + (n_{\alpha i}^y)^2 + (n_{\beta i}^x)^2 + (n_{\beta i}^y)^2 \} + \Gamma^1 n_{\alpha i}^x + \Gamma^2 n_{\alpha i}^y + 4\Gamma^{12} (n_{\alpha i}^x n_{\beta i}^x + n_{\alpha i}^y n_{\beta i}^y) + \Gamma^{25} n_{\beta i}^x + \Gamma^{51} n_{\beta i}^y \right]. \quad (4.26)$$

The term proportional to Γ^{12} does not contribute to AFM order and we will ignore it hereafter. Now it is convenient to introduce

$$n_{\alpha i}^{\pm} \equiv n_{\alpha i}^x \pm i n_{\alpha i}^y, \quad (4.27)$$

$$n_{\beta i}^{\pm} \equiv n_{\beta i}^x \pm i n_{\beta i}^y. \quad (4.28)$$

Using them, $\delta\mathcal{H}$ is written as

$$\begin{aligned} \delta\mathcal{H} = \frac{U\phi_{a0}}{2} \Big[& -\frac{1}{2}\Gamma^5(n_{\alpha i}^+n_{\alpha i}^- + n_{\beta i}^+n_{\beta i}^-) \\ & + \Gamma^+n_{\alpha i}^- + \Gamma^-n_{\alpha i}^+ + \Sigma^+n_{\beta i}^- + \Sigma^-n_{\beta i}^+ \Big], \end{aligned} \quad (4.29)$$

where

$$\Gamma^{\pm} = \frac{1}{\sqrt{2}}(\Gamma^1 \pm i\Gamma^2) = \sqrt{2} \begin{pmatrix} \sigma^+ & 0 \\ 0 & -\sigma^+ \end{pmatrix}, \quad (4.30)$$

$$\Sigma^{\pm} = \frac{1}{\sqrt{2}}(\Gamma^{25} \pm i\Gamma^{51}) = \sqrt{2} \begin{pmatrix} \sigma^- & 0 \\ 0 & -\sigma^- \end{pmatrix}. \quad (4.31)$$

Now we derive the effective action in a similar way as in Sec. 4.2. Computing the terms up to $\mathcal{O}((n_{\alpha i}^{\pm})^2, (n_{\beta i}^{\pm})^2)$, the effective action for the excitations is

$$S_{\text{eff}} \supset \frac{U\phi_{a0}^2}{2} \sum_{i\omega_n, \mathbf{k}} \sum_{\xi=\alpha, \beta} \tilde{n}_{\xi}^+(k) \tilde{n}_{\xi}^-(k) \tilde{\Gamma}_A^{\xi}(k), \quad (4.32)$$

where $\tilde{\Gamma}_M^{\xi}$ is given in Eq. (4.3) and $\tilde{\chi}_A^{\xi}(k)$ ($\xi = \alpha, \beta$) are given by

$$\tilde{\chi}_A^{\alpha}(k) = \frac{1}{2} \{ \chi_A(k; \Gamma^+, \Gamma^-) + \chi_A(k; \Gamma^-, \Gamma^+) \}, \quad (4.33)$$

$$\tilde{\chi}_A^{\beta}(k) = \frac{1}{2} \{ \chi_A(k; \Sigma^+, \Sigma^-) + \chi_A(k; \Sigma^-, \Sigma^+) \}. \quad (4.34)$$

Here the first term of $\tilde{\Gamma}_A^{\xi}$ is given by the term proportional to Γ^5 in Eq. (4.29). Diagrammatically it is a tadpole and we have found that it can be rewritten by using Eq. (3.11). As a result, it turns out to have the same structure as the amplitude modes.

We repeat the argument for the FM order. In this case, we take $\phi_{Ai} = \phi_{Bi} = \phi_{f0}/2$ to give the Hamiltonian H_U

$$\begin{aligned} H_U \supset \frac{U\phi_{f0}}{2} \sum_i c_i^{\dagger} \Big[& \Gamma^{12}n_{\alpha i}^z + \Gamma^{25}n_{\alpha i}^x + \Gamma^{51}n_{\alpha i}^y \\ & + \Gamma^5n_{\beta i}^z + \Gamma^1n_{\beta i}^x + \Gamma^2n_{\beta i}^y \Big] c_i. \end{aligned} \quad (4.35)$$

As seen, the Hamiltonian is given by a replacement $\Gamma^5 \leftrightarrow \Gamma^{12}$, $\Gamma^1 \leftrightarrow \Gamma^{25}$, $\Gamma^2 \leftrightarrow \Gamma^{51}$, and $\phi_{a0} \rightarrow \phi_{f0}$ in Eq. (4.24). Then the perturbative term $\delta\mathcal{H}$ in the Hamiltonian \mathcal{H} becomes,

$$\begin{aligned} \delta\mathcal{H} = \frac{U\phi_{f0}}{2} \Big[& -\frac{1}{2}\Gamma^{12}(n_{\alpha i}^+n_{\alpha i}^- + n_{\beta i}^+n_{\beta i}^-) \\ & + \Sigma^+n_{\alpha i}^- + \Sigma^-n_{\alpha i}^+ + \Gamma^+n_{\beta i}^- + \Gamma^-n_{\beta i}^+ \Big]. \end{aligned} \quad (4.36)$$

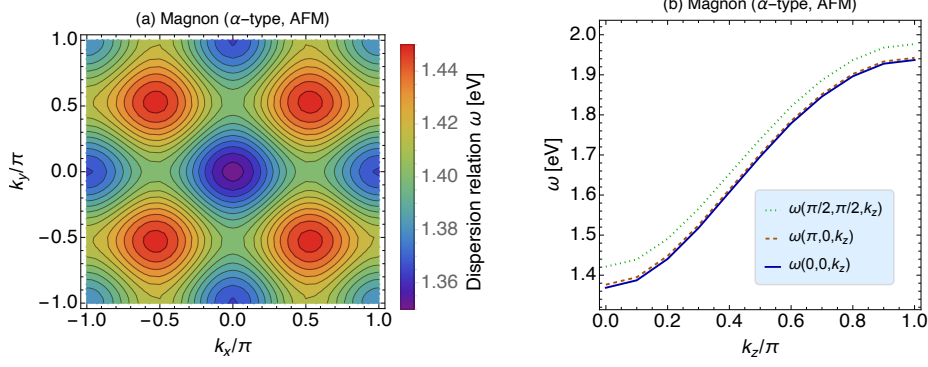


Figure 7. Dispersion relation for the α -type magnon under the AFM. (a) Contour of $\omega(k_x, k_y, 0)$. (b) $\omega(\mathbf{k})$ as function of k_z for various values of k_x, k_y . We take $U = 5$ eV and the other parameters are the same as Fig. 1.

Here we have omitted a term proportional to Γ^5 that is ineffective for the FM order. The effective action is then obtained by

$$S_{\text{eff}} \supset \frac{U\phi_{f0}^2}{2} \sum_{i\omega_n, \mathbf{k}} \sum_{\xi=\alpha, \beta} \tilde{n}_\xi^+(k) \tilde{n}_\xi^-(-k) \tilde{\Gamma}_F^\xi(k), \quad (4.37)$$

and

$$\tilde{\chi}_F^\alpha(k) = \frac{1}{2} \{ \chi_F(k; \Sigma^+, \Sigma^-) + \chi_F(k; \Sigma^-, \Sigma^+) \}, \quad (4.38)$$

$$\tilde{\chi}_F^\beta(k) = \frac{1}{2} \{ \chi_F(k; \Gamma^+, \Gamma^-) + \chi_F(k; \Gamma^-, \Gamma^+) \}. \quad (4.39)$$

The first term of $\tilde{\Gamma}_F^\xi$ comes from the term proportional to Γ^{12} . It corresponds to the tadpole diagram and it can be rewritten by using Eq. (3.12). Thus the structure is the same as $\tilde{\Gamma}_A^\xi$. With the FM order, the α -type and β -type of magnon corresponds to $n_{\alpha i}^\pm$ and $n_{\beta i}^\pm$, respectively, which are shown in Fig. 6 (bottom).

From the expressions of the effective action regarding magnons, i.e., Eqs. (4.32) and (4.37), the gap and dispersion relation of the magnon is given by

$$\tilde{\Gamma}_M^\xi(i\omega_n = \omega + i\delta, \mathbf{k}) = 0 \quad (\xi = \alpha, \beta, \quad M = A, F). \quad (4.40)$$

Now we show the numerical results of the dispersion relation of the magnons. Fig. 7 shows a plot of the dispersion relation regarding the α -type magnon under the AFM order. We have found the dispersion relation $\omega(\mathbf{k})$ is minimized at $\mathbf{k} = \mathbf{0}$. On the other hand, there are additional quasi-degenerate values of $\omega(\mathbf{k})$ at $\mathbf{k} = (\pi, 0, 0), (0, \pi, 0), (\pi, \pi, 0)$. The degeneracy is about 1%, compared to $\omega(\mathbf{0})$ and the curvatures of the wavenumbers are positive at the \mathbf{k} s. Therefore we expect four different stable configurations of the magnon. The excitation energy is found to be around eV.⁸

⁸When we derive the effective action for those configurations of magnon, we need to expand $\tilde{\Gamma}_A^\alpha(\omega, \mathbf{k})$ around each wavenumber, i.e., $\mathbf{k} = (\pi, 0, 0), (0, \pi, 0), (0, \pi, \pi)$.

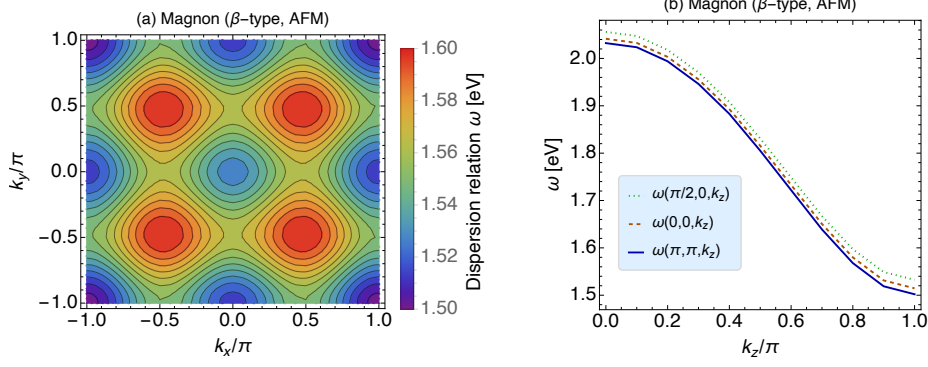


Figure 8. Same as Fig. 7 but for β -type magnon under the AFM. (a) Contour of $\omega(k_x, k_y, \pi)$. (b) $\omega(\mathbf{k})$ as function of k_z for various values of k_x, k_y .

Fig. 8 shows the dispersion relation for the β -type magnon under the AFM order. For the excitation similar result to the α -type is obtained but with a different configurations; we have found $\omega(\mathbf{k})$ has the minimum at $\mathbf{k} = (\pi, \pi, \pi)$, and cross values are found at $\mathbf{k} = (0, 0, \pi), (\pi, 0, \pi), (0, \pi, \pi)$ with a degeneracy of around 1%. The energy scale turns out to be the same as the α -type one, i.e., $\mathcal{O}(\text{eV})$.

It is worth discussing the origin of the gap of the magnons. Let us consider the α -type magnon under the AFM at zero temperature. Assuming that the expansion around $\omega = 0$ is valid, we get the stiffness and mass of the magnon as (see Appendix D for the derivation)

$$J'_\alpha = \int \frac{d^3\ell}{(2\pi)^3} \frac{2d^2 - d_1^2 - d_2^2}{8d^5}, \quad (4.41)$$

$$J'_\alpha m'^2_\alpha = \int \frac{d^3\ell}{(2\pi)^3} \frac{d_1^2 + d_2^2}{2d^3}. \quad (4.42)$$

It is clear that magnon is gapped at the zero temperature. From the expression, we see that gap is typically $\mathcal{O}(\text{eV})$, which is consistent with the numerical result shown in Fig. 7. The typical scale is the same as the AFM-type amplitude mode under the AFM. However, the parameter dependence is different; in the $U \rightarrow \infty$ limit, $J'_\alpha \propto \text{eV}^3/U^3$ and $J'_\alpha m'^2_\alpha \sim A_2^2 \text{eV}^2/U^3$ leads to $m'_\alpha \sim A_2$. Therefore, the gap remains to be $\mathcal{O}(A_2)$ even if U is much larger. We have also confirmed this numerically.

Based on the above argument, we expect that the gap of the magnon becomes zero when $d_1, d_2 \rightarrow 0$. This can be confirmed without the expansion with respect to ω ; considering the zero wavenumber and taking the limit at the zero temperature, Eq. (4.40) with $M = A$ and $\xi = \alpha$ gives rise to

$$1 - \frac{U}{2N} \sum_\ell \frac{1}{d} \frac{1}{1 - \omega^2/(4d^2)} = 0. \quad (4.43)$$

Recalling Eq. (3.11), it is easy to find $\omega = 0$ is the solution to satisfy the gap equation. Therefore nonzero d_1 and d_2 (or A_2) are the origin of the α -type magnon gap under the AFM. This can be understood by considering the symmetry breaking of the system. When

$d_1 = d_2 = 0$, $\text{SO}(3)$ symmetry in the $\vec{\phi}_{Ai} - \vec{\phi}_{Bi} \equiv 2\vec{\phi}_{ai}$ space is restored. Under the AFM order, the nonzero $\vec{\phi}_{ai} = (0, 0, \phi_{a0})$ breaks the $\text{SO}(3)$ to $\text{SO}(2)$. Consequently two massless Nambu-Goldstone bosons appear, which correspond to n_{ai}^\pm . See Appendix E for more detail.

Since we already have identified Nambu-Goldstone bosons, another excitation, β -type magnon under the AFM order, should be massive even if $d_1 = d_2 = 0$. In fact, by expanding $\tilde{\Gamma}_A^\beta(\omega, \mathbf{0})$ around $\omega = 0$, the stiffness and mass are given by

$$J'_\beta = \int \frac{d^3\ell}{(2\pi)^3} \frac{2d_5^2 + d_1^2 + d_2^2}{8d^5}, \quad (4.44)$$

$$J'_\beta m'^2_\beta = \int \frac{d^3\ell}{(2\pi)^3} \frac{2d_0^2 - d_1^2 - d_2^2}{2d^3}. \quad (4.45)$$

Thus a finite mass (or gap) should appear even if $d_1, d_2 \rightarrow 0$.

The results for α -type and β -type magnons under the FM state are similarly computed. It is found that qualitative features of the α -type and β -type ones are the same as the β - and α -types under the AFM order, respectively. Typical energy scale of the excitations are a bit smaller but they are $\mathcal{O}(\text{eV})$. See their plots in Appendix F.

To summarize this section, we have formulated the effective actions of the amplitude modes and magnons under both the AFM and FM orders. Each mode has two types; the amplitude mode has AFM- and FM-types and the magnon has the α - and β -types. From the effective action, we have computed the dispersion relations for all excitations. Among them, the AFM-type amplitude mode is identified as the ‘axionic’ quasi-particle. We have found that the mass of ‘axion’ coincides with the gap and it is derived more precisely compared to the past works. The typical energy scale turns out to be eV and the other excitations have the same scale.

5 Implication to axion search

As seen in Sec. 4.2, the ‘axionic’ excitation corresponds to the AFM-type amplitude mode (up to normalization of the field) under the AFM, and it is shown its mass (or gap) m_a is given by $U\phi_{a0}$. On the other hand, the energy bands of the electrons of the magnetic TIs are computed by the first-principles calculation. For $\text{Mn}_2\text{Bi}_2\text{Te}_5$, as an example, Ref. [13] shows that the gap of the electrons under the AFM order is $\mathcal{O}(10\text{-}10^2)$ meV. With this knowledge, we discuss the possibility of the axion detection by using the interaction of the ‘axion’ with the electromagnetic fields.

The ‘axion’ field θ has an $\mathbf{E} \cdot \mathbf{B}$ coupling in the Lagrangian [9]:

$$\mathcal{L}_{EB} = -\frac{\alpha}{4\pi}\theta F_{\mu\nu}\tilde{F}^{\mu\nu} = \frac{\alpha}{\pi}\theta \mathbf{E} \cdot \mathbf{B}, \quad (5.1)$$

where α is the fine-structure constant and $F_{\mu\nu}$ is the field strength of the electromagnetism.⁹ $\tilde{F}^{\mu\nu}$ is the dual of $F_{\mu\nu}$, defined as $\tilde{F}^{\mu\nu} = \frac{1}{2}\epsilon^{\mu\nu\rho\sigma}F_{\rho\sigma}$ ($\epsilon^{\mu\nu\rho\sigma}$ is the Levi-Civita symbol with

⁹ μ, ν, ρ, σ are the Lorentz indices that are 0, 1, 2, 3.

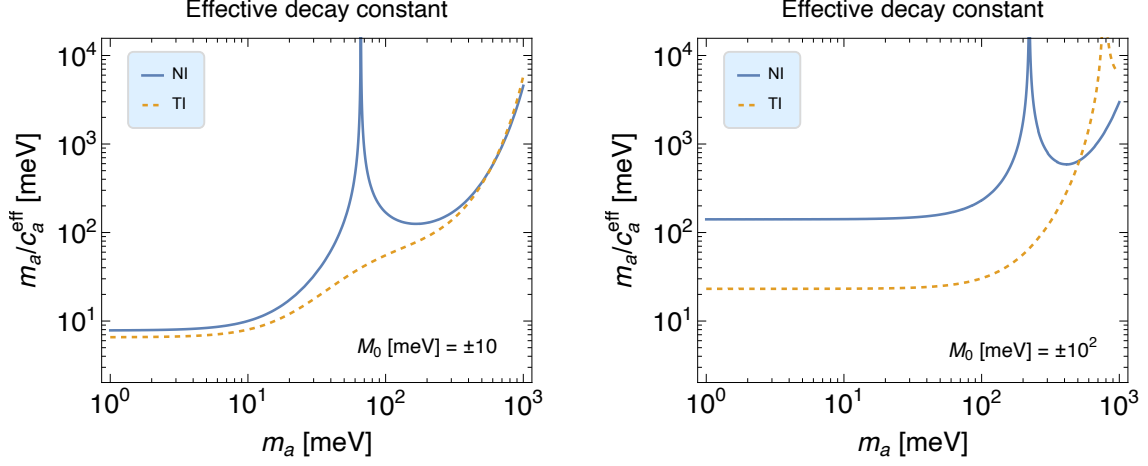


Figure 9. Effective decay constant m_a/c_a^{eff} as function of gap m_a of the amplitude mode. $M_0 [\text{meV}] = \pm 10$ (left) and $\pm 10^2$ (right) are taken, where positive (negative) M_0 corresponds to the NI (TI) phase. The other parameters (A_1 , A_2 , B_1 and B_2) are the same as Fig. 1.

$\epsilon^{0123} = +1$) and θ is related to the model parameters of the 3D TIs as [9]

$$\theta = \frac{1}{4\pi} \int d^3k \frac{2d + d_4}{(d + d_4)^2 d^3} \epsilon^{ijkl} d_i \partial_{k_x} d_j \partial_{k_y} d_k \partial_{k_z} d_l, \quad (5.2)$$

with i, j, k, l being 1, 2, 3, and 5.

Recalling that the effective action for the AFM-type amplitude mode under the AFM is given in Eq. (4.16), we define a canonically normalized field $\delta\hat{\phi}_a$:

$$\frac{U}{2} \sqrt{J} \delta\phi_a \equiv \frac{1}{\sqrt{2}} \delta\hat{\phi}_a. \quad (5.3)$$

Therefore, using

$$\begin{aligned} \delta\theta &= \frac{\partial\theta}{\partial d_5} \delta d_5 \\ &= \frac{\partial\theta}{\partial d_5} \frac{U}{2} \delta\phi_a \\ &= \frac{\partial\theta}{\partial \ln d_5} \sqrt{\frac{2}{J}} \frac{1}{m_a} \delta\hat{\phi}_a, \end{aligned} \quad (5.4)$$

the interaction term can be written in a form,

$$\mathcal{L}_{EB} \supset -\frac{\alpha}{4\pi} c_a^{\text{eff}} \frac{\delta\hat{\phi}_a}{m_a} F_{\mu\nu} \tilde{F}^{\mu\nu}, \quad (5.5)$$

where

$$c_a^{\text{eff}} = \left. \frac{\partial\theta}{\partial \ln \phi_a} \sqrt{\frac{2}{J}} \right|_{\phi_a = \phi_{a0}}. \quad (5.6)$$

Therefore, m_a/c_a^{eff} works as an effective “decay constant” for axion.¹⁰ In terms of a variable $g^{-1} = \partial\theta/\partial m_5$ (or $\partial\theta/\partial d_5$ in our notation) in the literature [9, 37], it is given by

$$g^2 J = \frac{1}{2} \left(\frac{m_a}{c_a^{\text{eff}}} \right)^2. \quad (5.7)$$

Or it is equivalent to f_Q used in Ref. [4], i.e.,

$$f_Q = \frac{m_a}{c_a^{\text{eff}}}. \quad (5.8)$$

We plot the effective decay constant of the amplitude mode as function of m_a in Fig. 9. Here we have used the fact that the AFM order parameter ϕ_{a0} becomes nonzero continuously as U increases shown in Sec. 3. Therefore m_a can take any value from zero to U if the value of U is properly chosen. In the plot the results for the NI and TI phases are given by taking $M_0 = \pm 10, \pm 10^2$ meV for comparison. Here we note that the enhancement point corresponds to a root of c_a^{eff} . While the results of the NI and TI are similar for $M_0 = \pm 10$ meV, those with $M_0 = \pm 10^2$ meV are different. This quantitative difference comes from the 3D TI model, which will be discussed below. To put it simply, we found that the effective coupling is $\mathcal{O}(10\text{--}10^2)$ meV for $m_a \lesssim 100$ meV.

Ref. [4], which proposes the axion detection using ‘axion’ in the magnetic TIs, claims that the effective decay constant f_Q is about 190 eV, based on Ref. [9]. However, this is larger than our result by $\mathcal{O}(10^3\text{--}10^4)$. Let us see this more closely. In Ref. [9], they use a variable $b^2 \equiv \alpha^2 B_0^2 / 2\pi^2 \epsilon g^2 J$,¹¹ where $B_0 = 2$ T and $\epsilon = 100$, and estimate b as $b = 0.5$ meV. Using this relation, $f_Q = \sqrt{2g^2 J}$ can be calculated as 180 eV, which is close to the value given in Ref. [4]. Namely, the estimate of $b = 0.5$ meV in Ref. [9] indicates $\sqrt{g^2 J} \simeq 130$ eV. One may think that this discrepancy comes from another choice of the input parameters. However, such a possibility is unlikely from an analytic estimation below.

Let us focus on the case where $d_5 (= m_a/2) = \mathcal{O}(1)$ meV that is considered in Ref. [9]. To take an analytic approach, we consider the Dirac model instead of the 3D TI model. The Dirac model is given by expanding the 3D TI model around $\mathbf{k} = 0$. See Eq. (F.2) for the explicit form. It is empirically known that physical properties of the excitation near its gap are unchanged in either model. Thus, the Dirac model can be a good tool to understand the physical behavior analytically. Since this scale is much smaller than the energy scale of the electrons, θ in the Dirac model is approximately given by [10]

$$\theta \sim \frac{\pi}{2} [1 - \text{sgn}(M_0)] \text{sgn}(d_5) + \frac{d_5}{M_0}, \quad (5.9)$$

which leads to

$$g^{-1} \sim 1/M_0. \quad (5.10)$$

In addition, J is estimated as

$$J \simeq \int \frac{d^3 \ell}{(2\pi)^3} \frac{1}{4d_0^3} \sim \mathcal{O}(0.1\text{--}1). \quad (5.11)$$

¹⁰Be aware that there is an additional factor of $\alpha/(4\pi)$ in the $\delta\hat{\phi}_a F\tilde{F}$ coupling.

¹¹We have changed the expression in the literature to one in the natural unit.

The estimation above is also checked numerically. Therefore, we get

$$\frac{m_a}{\sqrt{2}c_a^{\text{eff}}} = \sqrt{g^2 J} \sim \mathcal{O}(0.1 - 1) \times |M_0|, \quad (5.12)$$

for $d_5 \sim \text{meV}$. This estimation is roughly consistent with the results shown in Fig. 9. For a reference, we have computed the effective decay constant with the Dirac model. See Appendix F for the plots of the results. We note that $|M_0|$ does not exceed the typical energy scale of the electron, i.e., $\mathcal{O}(\text{eV})$. This is the reason that the value $\sqrt{g^2 J} \sim 10^2 \text{ eV}$ is unlikely.¹²

A careful reader may be curious about the result of the TI case with $M_0 = -100 \text{ meV}$, which is relatively smaller than the rough estimation. The suppression of the effective decay constant compared to the NI case can be understood from Eq. (5.2). In this expression, only d_4 changes with the sign of M_0 , and d_4 is slightly suppressed when $M_0 < 0$ compared to $M_0 > 0$ case with B_1 and B_2 unchanged. As a result, θ tends to be slightly enhanced. Therefore, since $\partial\theta/\partial d_5$ is also enhanced, m_a/c_a^{eff} is suppressed. (On the other hand, for the case of $|M_0| = 10 \text{ meV}$, the asymptotic value of the effective decay constant does not depend on the sign of M_0 because the contribution of M_0 itself in d_4 is smaller.)

As mentioned before, the enhancement of the effective decay constant is due to the root of c_a^{eff} . In general the root exists for both the NI and TI cases and the location of the root depends on the parameter. Therefore, although there are quantitative differences in the behavior of effective coupling constants in NI and TI, depending on the parameters, there is no qualitative difference in physical properties.

Some readers would be interested in the estimation of the axion mass and the effective coupling by using the result of the first-principles calculation. Applying the result of Ref. [13] to the model parameters, i.e., $A_1 = 1.2 \text{ eV}$, $A_2 = 2.6 \text{ eV}$, $B_1 = -0.38 \text{ eV}$, $B_2 = -2.1 \text{ eV}$, $M_0 = -0.024 \text{ eV}$, we obtain $\phi_{a0} \simeq 1.5 \times 10^{-3}$ and $m_a \simeq 20 \text{ meV}$. The effective decay constant is given by $m_a/c_a^{\text{eff}} \simeq 3 \text{ meV}$. This result is qualitatively the same as $M_0 = -10 \text{ meV}$ case in Fig. 9. Additionally, the stability of the excitation is checked. See Fig. 14 for the dispersion relation in Appendix F. Here we point out possible uncertainty that the determination of the parameter from the first-principles calculation has. The first-principles calculation provides the band structure of the material. On the other hand, the parameters of the model of the magnetic topological insulators can only be determined by the fitting of the band structure. For example, the band gap determined by first-principles calculation gives the value of $\sqrt{d_5^2 + M_0^2}$, not the respective values of d_5 and M_0 . This difficulty comes from the magnetic order. If we consider Bi_2Se_3 , d_5 is zero due to the time reversal invariance from the crystal structure. As a consequence, M_0 is determined by the value of the band gap. In the present case, however, we consider the state of the antiferromagnetic order and the above argument does not apply. Since d_5 and M_0 play an important role in determining the axion mass and the effective coupling constant, this indeterminacy will likely strongly affect them.

To summarize this section, with the estimate (5.12) and $M_0 = 10 \text{ meV}$, the signal strength of the axion detection proposal given in Ref. [4] is enhanced by about four orders

¹²Ref. [35] indicates $f_Q \sim 30 \text{ eV}$, which is still much larger than the present estimation.

of magnitude, which drastically improves the sensitivity of the detection if the technique claimed in the literature is feasible. In addition, we have shown that the effective decay constant is qualitatively topology-independent. This fact will encourage selecting suitable material for axion search from a broad perspective.

Finally, we point out a possible interaction of the magnon with the electromagnetic fields. For instance, since α -type magnon appears as Γ^5 term, we have

$$\begin{aligned}\delta\theta &= \frac{\partial\theta}{\partial d_5} \delta d_5 \\ &= \frac{\partial\theta}{\partial d_5} \left(-\frac{U}{4} \phi_{a0} n_\alpha^+ n_\alpha^- \right) \\ &= -\frac{\partial\theta}{\partial \ln d_5} \frac{2}{J_\alpha} \frac{1}{m_a^2} \hat{n}_\alpha^+ \hat{n}_\alpha^-, \end{aligned} \quad (5.13)$$

where we have defined a canonically normalized field for the α -type magnon under the AFM order as

$$\frac{U\phi_{a0}}{2} \sqrt{J_\alpha} n_\alpha^\pm \equiv \hat{n}_\alpha^\pm. \quad (5.14)$$

Then the interaction with the electromagnetic field is

$$\mathcal{L}_{EB} \supset -\frac{\alpha}{4\pi} c_\alpha^{\text{eff}} \frac{\hat{n}_\alpha^+ \hat{n}_\alpha^-}{m_a^2} F_{\mu\nu} \tilde{F}^{\mu\nu}, \quad (5.15)$$

where

$$c_\alpha^{\text{eff}} = \frac{\partial\theta}{\partial \ln \phi_a} \frac{2}{J_\alpha} \Big|_{\phi_a=\phi_{a0}}. \quad (5.16)$$

The interaction indicates that two magnons are excited under the electromagnetic fields, which can be another interesting signal for the axion detection. However, we have found that the magnon tends to dissipate when its mass is below $\mathcal{O}(\text{eV})$. This is true when we use the parameters given by Ref. [13]. Therefore, it would be challenging to detect such excitations. Instead, there may be a possibility of finding a relic of the dissipation of the two magnons, which is induced by the axion. We leave it for future investigation.

6 Conclusion

We have investigated possible excitations in the effective model of 3D magnetic topological insulators and discussed their impact on the axion detection. The model consists of the 3D effective model of TIs and the Hubbard term. In the current study we focus on the zero temperature case. Computing the effective potential from the grand potential, the AFM and FM orders are found. Both orders are triggered by a large value of U , which is a dimensionful coefficient of the Hubbard term. It turns out that the AFM state is lower energy than the FM, i.e., the AFM is the global minimum of the system. The order parameter ϕ_{a0} of the AFM appears continuously from zero, meanwhile that of the FM state turns out to emerge discontinuously.

Under the magnetic orders, we have derived the effective action for possible magnetic excitations. The magnetic excitations are classified by amplitude mode and magnon. Furthermore, the amplitude mode and magnon have two types: AFM/FM-types and α/β -types. We consider those four excitations under both the AFM and FM states, that are in total eight magnetic excitations. We found that the effective actions for all excitations are given by the inverse propagator that is composed of the dynamical susceptibility. The formulation provides not only the dispersion relation and the correspondence between the gap and mass of the excitations but also a criterion for the stability and validity of the effective description of the excitations.

With the formalism, we have found the AFM-type amplitude mode under the AFM is stable and the other amplitude modes tend to dissipate. The gap (or mass) of the AFM-type amplitude mode under the AFM is given by $m_a = U\phi_{a0}$. Namely, the gap is typically U (\sim eV) for a saturated magnetization $\phi_{a0} \sim 1$. On the other hand, it can be suppressed when $\phi_{a0} \ll 1$.

The four magnons turn out to be stable and their typical mass scale is $\mathcal{O}(\text{eV})$. For stable magnons, we have found there are several quasi-degenerate configurations. Taking the α -type magnon under the AFM as an example, the states with wavenumber $(\pi, 0, 0)$, $(0, \pi, 0)$, and $(\pi, \pi, 0)$ are found to be stable in addition to one with $(0, 0, 0)$. On the other hand, we discovered the magnon tends to dissipate for $\phi_{a0} \lesssim 1$.

We are especially interested in the AFM-type amplitude modes because they relate to ‘axionic’ quasi-particle and axion detection. First of all, we have identified ‘axion’ as the AFM-type amplitude mode under the AFM. Besides, we have determined its mass and the effective coupling to the electromagnetic fields more accurately than the past works. Since the mass ranges from zero to U , it is possible to consider a situation where the mass is less than $\mathcal{O}(10^2)$ meV. In the scale, the effective decay constant of ‘axion,’ determined by the effective coupling and the mass, turns out to be $\mathcal{O}(10-10^2)$ meV. This value is about three to four orders of magnitude smaller than the previous estimate, which has a significant impact on the proposal of the axion detection using ‘axion’ in the magnetic TIs. We also point out that the nature of ‘axion’ is insensitive to the topology of the magnetic insulators, i.e., topological phase or normal phase.

The suppression of the effective decay constant of ‘axion’ is good news for the axion detection. In addition, the topological nature of the materials is unnecessary to utilize ‘axion’ for the search. The magnon under the AFM state is another possibility to access to axion. Therefore, it is worth pursuing materials from broader candidates by studying their magnetic states and collective excitations that are suitable for the axion search. On the theoretical side, extensions of the model and simulations by the first-principles calculation would be the next step to further investigation of the magnetic excitations. We will leave it for future study.

Acknowledgments

We are grateful to Makoto Naka for valuable discussions in the early stage of this project. We also thank Fumiyuki Ishii, Kaiki Shibata, and Naoya Yamaguchi for useful discussion.

This work was supported by JSPS KAKENHI Grant Numbers JP18H05542, JP20H01894, and JSPS Core-to-Core Program Grant No. JPJSCCA20200002 (KI), and JST CREST, Grant No. JPMJCR18T2 (KN).

A Notation

We summarize the Gamma matrices and the notation for the wavefunction and Green's function we use in this paper.

A.1 Gamma matrices

In this study we mainly use the Gamma matrices in the so-called sublattice basis. In the basis the Gamma matrices Γ^a ($a = 1, \dots, 5$) are defined as

$$\begin{aligned}\Gamma^1 &= \begin{pmatrix} \sigma^1 & 0 \\ 0 & -\sigma^1 \end{pmatrix}, \quad \Gamma^2 = \begin{pmatrix} \sigma^2 & 0 \\ 0 & -\sigma^2 \end{pmatrix}, \quad \Gamma^3 = \begin{pmatrix} 0 & -i\mathbf{1} \\ i\mathbf{1} & 0 \end{pmatrix}, \\ \Gamma^4 &= \begin{pmatrix} 0 & -\mathbf{1} \\ -\mathbf{1} & 0 \end{pmatrix}, \quad \Gamma^5 = \begin{pmatrix} \sigma^3 & 0 \\ 0 & -\sigma^3 \end{pmatrix}.\end{aligned}\tag{A.1}$$

Γ^5 can also be written by $\Gamma^5 = -\Gamma^1\Gamma^2\Gamma^3\Gamma^4$. In addition, we define

$$\Gamma^{ab} = \frac{1}{2i} [\Gamma^a, \Gamma^b].\tag{A.2}$$

The explicit form of Γ^{25} , Γ^{51} , and Γ^{12} are

$$\Gamma^{25} = \begin{pmatrix} \sigma^1 & 0 \\ 0 & \sigma^1 \end{pmatrix}, \quad \Gamma^{51} = \begin{pmatrix} \sigma^2 & 0 \\ 0 & \sigma^2 \end{pmatrix}, \quad \Gamma^{12} = \begin{pmatrix} \sigma^3 & 0 \\ 0 & \sigma^3 \end{pmatrix}.\tag{A.3}$$

The operators Γ^a ($a = 1, 2, 5$) and Γ^{ab} ($ab = 25, 51, 12$) represent the AFM and FM order parameters of (x, y, z) directions, respectively. Especially Γ^{ab} ($ab = 25, 51, 12$) correspond to the spin operator in the Dirac Gamma matrices in particle physics.

Recalling the Dirac Gamma matrices, one may wonder that Γ^{ab} ($ab = 23, 31, 12$) should be used instead of Eq. (A.3). This confusion is due to different representations of the Gamma matrices. Namely, Γ^a ($a = 1, 2, 3, 5$) can be replaced each other by a unitary transformation. For instance, a unitary transformation $\Gamma^a \rightarrow \Gamma^{a'} = U\Gamma^a U^\dagger$ by a unitary matrix

$$U = \frac{1}{\sqrt{2}} \begin{pmatrix} 1 & -i\sigma^1 \\ -i\sigma^1 & 1 \end{pmatrix},\tag{A.4}$$

which is U_3 in Ref. [38], gives $\Gamma^3 \rightarrow \Gamma^5$, $\Gamma^5 \rightarrow -\Gamma^3$, and the others remain. This indicates that we can construct a representation of the Lorentz group from three matrices out of four ones. In the sublattice basis, we can use Γ^1 , Γ^2 , and Γ^5 . Let us see this explicitly below.

To begin with, we define J_i ($i = 1, 2, 3$) and K_i ($i = 1, 2, 3$) as

$$J_i = \frac{1}{4} \epsilon_{iab} \Gamma^{ab}, \quad K_i = \frac{i}{4} \Gamma^{4i},\tag{A.5}$$

where ϵ_{iab} is the Levi-Civita symbol and indices a and b take 1, 2 or 5, such as $J_1 = \Gamma^{25}/2$, $J_2 = \Gamma^{51}/2$ etc. Then they obey the following commutation relation:

$$[J_i, J_j] = i\epsilon_{ijk}J_k, [K_i, K_j] = -i\epsilon_{ijk}J_k, [J_i, K_j] = i\epsilon_{ijk}K_k, \quad (\text{A.6})$$

which shows that J_i and K_i are the generators of the Lorentz transformation. Especially J_i are the operators for the rotational transformations. Let us focus on J_1 as an example. An operator for a finite θ rotation along $i = 1$, i.e., x axis, is given by

$$S = e^{i\frac{\theta}{2}\Gamma^{25}} = \cos \frac{\theta}{2} + i\Gamma^{25} \sin \frac{\theta}{2}, \quad (\text{A.7})$$

Then we obtain

$$S^{-1}\Gamma^1 S = \Gamma^1, \quad (\text{A.8})$$

$$S^{-1}\Gamma^2 S = \Gamma^2 \cos \theta + \Gamma^5 \sin \theta, \quad (\text{A.9})$$

$$S^{-1}\Gamma^5 S = -\Gamma^2 \sin \theta + \Gamma^5 \cos \theta. \quad (\text{A.10})$$

Therefore, it is confirmed that J_i are the generators for rotation in three dimensional space with axes $i = 1, 2, 5$. Since the generators of the rotational transformation are the spin operators up to a factor, Γ^{25} , Γ^{51} , and Γ^{12} are introduced for the FM order. Accordingly, Γ^1 , Γ^2 , and Γ^5 are used for the AFM order.

We note that the above calculation of the rotational transformation of the Gamma matrices is just to show an example that Eq. (A.5) are the generators of the Lorentz transformation. This has nothing to do with the discrete symmetry of the crystal structure. The 3D TI model has the time-reversal symmetry, space inversion symmetry, and three-fold rotation symmetry along the z axis [9, 29, 30], except for Γ^5 term. Each Gamma matrix is the representation of the symmetries [30] and the unitary transformation of the Gamma matrices does not change the physical interpretation of each Γ^a .

A.2 Wavefunction and Green's function

In a finite temperature the wavefunction Φ_i and the Green's function G is Fourier expanded as

$$\Phi_i(\tau) = \frac{1}{\sqrt{\beta N}} \sum_{i\omega_n, \mathbf{k}} \tilde{\Phi}(i\omega_n, \mathbf{k}) e^{-i\omega_n \tau + i\mathbf{k} \cdot \mathbf{x}_i}, \quad (\text{A.11})$$

$$G(x_i - x_j) = \frac{1}{\beta N} \sum_{i\omega_n, \mathbf{k}} \tilde{G}(i\omega_n, \mathbf{k}) e^{-i\omega_n(\tau_i - \tau_j) + i\mathbf{k} \cdot (\mathbf{x}_i - \mathbf{x}_j)}, \quad (\text{A.12})$$

where \mathbf{x}_i shows the location of the cite i and $x_i = (\tau_i, \mathbf{x}_i)$. Φ_i includes c_i , $\delta\phi_{ai}$, $\delta\phi_{fi}$, and $n_{\alpha i}^{\pm}$, $n_{\beta i}^{\pm}$. Regarding the Green's function, we change the definition of G according to the magnetic order of the system. For instance, if there is no magnetic order, then we choose $G^{-1} = -\partial_{\tau} - \mathcal{H}^{\text{TI}}$, leading to $\tilde{G} = (-i\omega_n + d_0)^{-1}$.

B Dynamical susceptibility

In this section, we give the expression for the dynamical susceptibility used in the numerical calculation. We have introduced eight kinds of susceptibilities and they can be written in a generic form as

$$\chi_M(k; O_1, O_2) = -\frac{1}{\beta N} \sum_{i\omega_\ell, \ell} \text{Tr}[\tilde{G}_M(\ell) O_1 \tilde{G}_M(\ell + k) O_2], \quad (\text{B.1})$$

where O_1 and O_2 stand for the Gamma matrices, such as Γ^a , Γ^\pm , or Σ^\pm . Recalling that $\tilde{G}_M(\ell) = (-i\omega_\ell + \mathcal{H}_\ell)^{-1}$, $\tilde{G}_M(\ell)$ can be diagonalized by a unitary matrix as

$$U_\ell^\dagger \tilde{G}_M(\ell) U_\ell = \tilde{G}_M(\ell)_{\text{diag}}, \quad (\text{B.2})$$

where $\tilde{G}_M(\ell)_{\text{diag}}$ is a diagonal matrix and $\tilde{G}_M^{-1}(\ell) = \text{diag}(-i\omega_\ell + E_{1\ell}, -i\omega_\ell + E_{2\ell}, -i\omega_\ell + E_{3\ell}, -i\omega_\ell + E_{4\ell})$. Similarly, $\tilde{G}_M(\ell + k)$ is diagonalized as

$$U_{\ell+k}^\dagger \tilde{G}_M(\ell + k) U_{\ell+k} = \tilde{G}_M(\ell + k)_{\text{diag}}. \quad (\text{B.3})$$

Then the trace part is

$$\begin{aligned} \text{Tr}[\tilde{G}_M(\ell) O_1 \tilde{G}_M(\ell + k) O_2] &= \text{Tr}[\tilde{G}_M(\ell)_{\text{diag}} O'_1 \tilde{G}_M(\ell + k)_{\text{diag}} O'_2] \\ &= \sum_{i,j} \frac{1}{i\omega_n - E_{i\mathbf{k}}} \frac{1}{i\omega_n + i\omega_\ell - E_{j\ell+k}} (O'_1)_{ij} (O'_2)_{ji} \end{aligned} \quad (\text{B.4})$$

where

$$O'_1 = U_\ell^\dagger O_1 U_{\ell+k}, \quad (\text{B.5})$$

$$O'_2 = U_{\ell+k}^\dagger O_2 U_\ell. \quad (\text{B.6})$$

Summing over $i\omega_\ell$, we finally get

$$\chi_M(i\omega_n, \mathbf{k}; O_1, O_2) = - \sum_{\ell} \sum_{i,j} \frac{(O'_1)_{ij} (O'_2)_{ji}}{i\omega_n + E_{j\ell+k} - E_{i\mathbf{k}}} (n_F(E_{i\ell}) - n_F(E_{j\ell+k})). \quad (\text{B.7})$$

C Dynamical susceptibility under AFM at zero temperature

With the AFM order at zero temperature, the susceptibility can be derived analytically. In the limit $\beta^{-1} \sum_{i\omega_\ell}$ is replaced by $\int d\ell_E^0 / (2\pi)$ where $\omega_\ell = \ell_E^0$. We list the results below:

$$\tilde{\chi}_A^a(i\omega_n = \omega, \mathbf{k}) = \frac{2}{N} \sum_{\ell} \frac{df + \sum_{a=1}^5 d_a f_a - 2d_5^2}{P}, \quad (\text{C.1})$$

$$\tilde{\chi}_A^f(i\omega_n = \omega, \mathbf{k}) = \frac{2}{N} \sum_{\ell} \frac{df - \sum_{a=1}^5 d_a f_a + 2(d_1 f_1 + d_2 f_2)}{P}, \quad (\text{C.2})$$

$$\tilde{\chi}_A^\alpha(i\omega_n = \omega, \mathbf{k}) = \frac{2}{N} \sum_{\ell} \frac{df + \sum_{a=1}^5 d_a f_a - (d_1 f_1 + d_2 f_2)}{P}, \quad (\text{C.3})$$

$$\tilde{\chi}_A^\beta(i\omega_n = \omega, \mathbf{k}) = \frac{2}{N} \sum_{\ell} \frac{df - \sum_{a=1}^5 d_a f_a + (2d_5^2 + d_1 f_1 + d_2 f_2)}{P}, \quad (\text{C.4})$$

where

$$P = df(d+f)\{1 - \omega^2/(d+f)^2\}. \quad (\text{C.5})$$

d_a and f_a ($a = 1-4$) depend on the wavenumber as $d_a = d_a(\ell)$ and $f_a = d_a(\ell + \mathbf{k})$ and $f_5 = d_5$. f is defined by $f = (\sum_{a=1}^5 f_a f_a)^{1/2}$.

D How to derive the effective action of the excitation at zero temperature

In this section we derive the effective action for the excitation in the continuum and zero temperature limit. Using the dynamical susceptibility, the effective (Euclidean) action for the excitation has a form (see Eqs. (4.10), (4.32) and (4.37)),

$$S_E = \frac{U\phi_0}{2} \sum_{i\omega, \mathbf{k}} \tilde{\eta}^*(k) \tilde{\eta}(-k) \tilde{\Gamma}(k), \quad (\text{D.1})$$

where η is the excitation ($\tilde{\eta}$ is the Fourier coefficient) and

$$\tilde{\Gamma}(k) \equiv 1 - \frac{U}{4} \tilde{\chi}_M(i\omega_n, \mathbf{k}). \quad (\text{D.2})$$

ϕ_0 is unity, ϕ_{a0}^2 , or ϕ_{f0}^2 , depending on the excitation. Since $\tilde{\Gamma}$ is the inverse of the two-point Green's function, the effective action can be derived by expanding it at the mass m ,

$$\begin{aligned} \tilde{\Gamma}(i\omega_n, \mathbf{k}) &= \frac{\partial \tilde{\Gamma}}{\partial (i\omega_n)^2} \Big|_{i\omega_n=m, \mathbf{k}=\mathbf{0}} ((i\omega_n)^2 - m^2) \\ &\quad + \sum_i \frac{\partial \tilde{\Gamma}}{\partial k_i^2} \Big|_{i\omega_n=m, \mathbf{k}=\mathbf{0}} k_i^2 + \dots \end{aligned} \quad (\text{D.3})$$

Here we have used the definition of the mass:

$$\tilde{\Gamma}(i\omega_n = m, \mathbf{0}) = 0. \quad (\text{D.4})$$

In the continuum coordinate space it can be written as

$$\begin{aligned} S_E &= \frac{U\phi_0}{2} \int^\beta d\tau \sum_i \eta^* \frac{U}{2} a^3 J (-\partial_\tau^2 + v_i^2 k_i^2 + m^2) \eta \\ &\rightarrow \frac{U\phi_0}{2} \int^\beta d\tau \int d^3x \eta^* \frac{U}{2} J (-\partial_\tau^2 + v_i^2 k_i^2 + m^2) \eta, \end{aligned} \quad (\text{D.5})$$

where we have retrieved the lattice size a to make the dimension of the action intact. J and v_i are the stiffness and velocity defined as

$$\frac{U}{2} a^3 J = - \frac{\partial \tilde{\Gamma}}{\partial (i\omega_n)^2} \Big|_{i\omega_n=m, \mathbf{k}=\mathbf{0}}, \quad (\text{D.6})$$

$$\frac{U}{2} a^3 J v_i^2 = \frac{\partial \tilde{\Gamma}}{\partial k_i^2} \Big|_{i\omega_n=m, \mathbf{k}=\mathbf{0}}. \quad (\text{D.7})$$

Using the real time ($t = -i\tau$), we get the (Minkowski) action as

$$iS_E \rightarrow S = \left(\frac{U}{2}\right)^2 \phi_0 J \int d^4x \eta^* (-\partial_t^2 + v_i^2 \partial_i^2 - m^2) \eta. \quad (\text{D.8})$$

Let us calculate the stiffness for the AFM-type amplitude mode in the AFM order. In this case, the mass is given by $U\phi_0$. Then

$$\begin{aligned} \frac{U}{2} a^3 J &= \frac{U}{2N} \sum_{\ell} \frac{d_0^2}{4d^5} \frac{1}{(1 - d_5^2/d^2)^2} \\ &\rightarrow J = \int \frac{d^3\ell}{(2\pi)^3} \frac{1}{4dd_0^2}. \end{aligned} \quad (\text{D.9})$$

In the previous works [9, 10], $\tilde{\Gamma}$ is expanded around $i\omega_n = 0$. Namely,

$$\tilde{\Gamma}_A^a(i\omega_n = \omega, \mathbf{0}) = \frac{U}{2N} \sum_{\ell} \left[\frac{d_5^2}{d^3} - \frac{d_0^2}{4d^5} \omega^2 + \mathcal{O}(\omega^4) \right]. \quad (\text{D.10})$$

As a result, we get

$$J^{\text{old}} = \int \frac{d^3\ell}{(2\pi)^3} \frac{d_0^2}{4d^5}, \quad (\text{D.11})$$

$$J^{\text{old}}(m_a^{\text{old}})^2 = \int \frac{d^3\ell}{(2\pi)^3} \frac{d_5^2}{d^3}. \quad (\text{D.12})$$

It is clear that the expansion around $\omega = 0$ in Eq. (D.10) is guaranteed if m_a^{old} is smaller than $2d$. If this condition is satisfied, then the expansion is valid and we expect $m_a^{\text{old}} \simeq m_a$. The discrepancy between the old results and the new ones is shown in Fig. 10. We found that they agree at around $(10^{-3} - 10)\%$ for $m_a \sim (\text{meV} - \text{eV})$. Therefore the old results are a good approximation for $m_a \lesssim \mathcal{O}(\text{eV})$.

Similarly, the stiffness for the α -type magnon with the AFM is

$$J_{\alpha} = \int \frac{d^3\ell}{(2\pi)^3} \frac{2d^2 - d_1^2 - d_2^2}{8d^3} \frac{1}{(1 - m_{\alpha}^2/(4d^2))^2}, \quad (\text{D.13})$$

where the mass m_{α} is given by $\tilde{\Gamma}_A^{\alpha}(i\omega_n = m_{\alpha}, \mathbf{0}) = 0$. On the other hand, if we expand $\tilde{\Gamma}_A^{\alpha}$ around $i\omega_n = 0$, i.e.,

$$\tilde{\Gamma}_A^{\alpha}(i\omega_n = \omega, \mathbf{0}) = \frac{U}{2N} \sum_{\ell} \left[\frac{d_1^2 + d_2^2}{2d^3} - \frac{2d^2 - d_1^2 - d_2^2}{8d^5} \omega^2 + \mathcal{O}(\omega^4) \right], \quad (\text{D.14})$$

we obtain

$$J'_{\alpha} = \int \frac{d^3\ell}{(2\pi)^3} \frac{2d^2 - d_1^2 - d_2^2}{8d^5}, \quad (\text{D.15})$$

$$J'_{\alpha} m_{\alpha}'^2 = \int \frac{d^3\ell}{(2\pi)^3} \frac{d_1^2 + d_2^2}{2d^3}. \quad (\text{D.16})$$

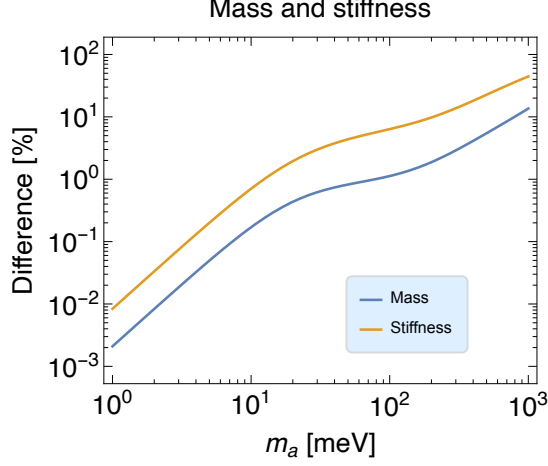


Figure 10. Comparison of the mass and stiffness of axionic excitation. $r_m = -(m_a - m_a^{\text{old}})/m_a$ and $r_J = (J - J^{\text{old}})/J$ are plotted as function of m_a . The other parameters are the same as Fig. 1.

E Symmetry of the Hamiltonian

To understand the appearance of the gapless modes, we use

$$\vec{\phi}_{ai} = (\vec{\phi}_{Ai} - \vec{\phi}_{Bi})/2, \quad (\text{E.1})$$

$$\vec{\phi}_{fi} = (\vec{\phi}_{Ai} + \vec{\phi}_{Bi})/2, \quad (\text{E.2})$$

in this section. The Hubbard term after the Stratonovich-Hubbard transformation gives,

$$H_U \rightarrow \frac{U}{2} \sum_i (\vec{\phi}_{ai}^2 + \vec{\phi}_{fi}^2) + \frac{U}{2} \sum_i c_i^\dagger [\vec{\phi}_{ai} \cdot \vec{\Gamma} + \vec{\phi}_{fi} \cdot \vec{\Sigma}] c_i, \quad (\text{E.3})$$

where we have introduced $\vec{\Gamma} = (\Gamma^1, \Gamma^2, \Gamma^5)$ and $\vec{\Sigma} = (\Gamma^{25}, \Gamma^{51}, \Gamma^{12})$. It can be seen that the rotational invariance of the Hubbard term is intact in the parameter space of magnetic orders, $\vec{\phi}_{ai}$ and $\vec{\phi}_{fi}$, which corresponds to $(\Gamma^1, \Gamma^2, \Gamma^5)$ space. See also Appendix A.1. This symmetry is broken by \mathcal{H}^{TI} , i.e., Γ^1 and Γ^2 terms that couple to the wavenumbers. To see the structure of the symmetry, we take $d_1 = d_2 = 0$ hereafter. In addition we consider a uniform magnetic configuration to study the magnons of the zero mode.

The Hamiltonian \mathcal{H} is given by

$$\begin{aligned} \mathcal{H} &= \mathcal{H}^{\text{MTI}} + \delta\mathcal{H} \\ &= \sum_{a=3}^4 d_a \Gamma^a + \frac{U}{2} (\vec{\phi}_a \cdot \vec{\Gamma} + \vec{\phi}_f \cdot \vec{\Sigma}). \end{aligned} \quad (\text{E.4})$$

and the energy eigenvalues are

$$\pm \sqrt{d_s^2 + \vec{\phi}_a^2 + \vec{\phi}_f^2 + 2\sqrt{\vec{\phi}_a \cdot \vec{\phi}_f + d_s^2(\vec{\phi}_a^2 + \vec{\phi}_f^2)}}, \quad (\text{E.5})$$

$$\pm \sqrt{d_s^2 + \vec{\phi}_a^2 + \vec{\phi}_f^2 - 2\sqrt{\vec{\phi}_a \cdot \vec{\phi}_f + d_s^2(\vec{\phi}_a^2 + \vec{\phi}_f^2)}}. \quad (\text{E.6})$$

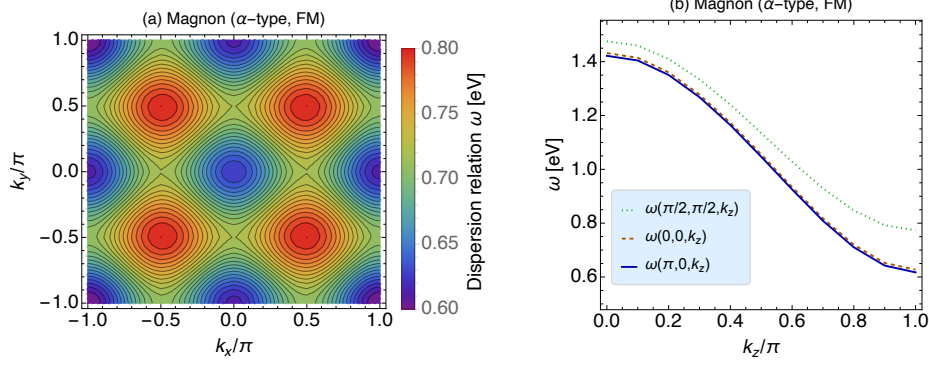


Figure 11. Dispersion relation for α -type magnon under the FM. (a) Contour of $\omega(k_x, k_y, \pi)$. (b) $\omega(\mathbf{k})$ as function of k_z for various values of k_x, k_y .

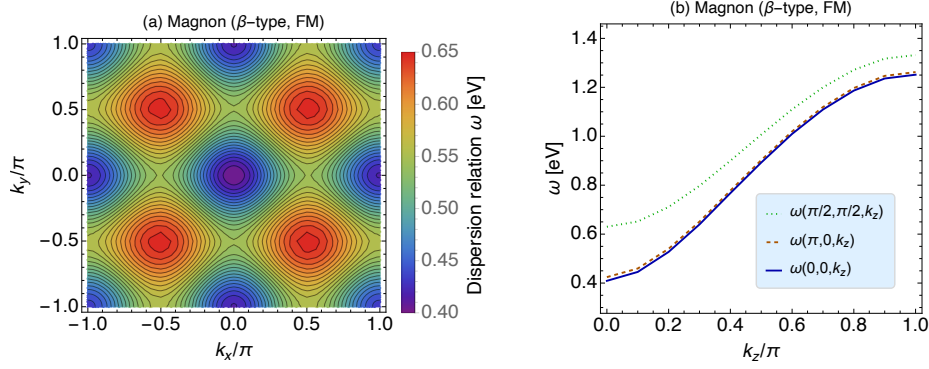


Figure 12. Same as Fig. 11 but for β -type magnon under the FM. (a) Contour of $\omega(k_x, k_y, 0)$. (b) $\omega(\mathbf{k})$ as function of k_z for various values of k_x, k_y . The other parameters are the same as Fig. 1.

The expression clearly shows that the system has $SO(3)$ symmetry. Under the AFM state, with $(\phi_{az}, \phi_{fz}) = (\phi_{a0}, 0)$, you can see that $SO(3)$ is broken to $SO(2)$. Therefore, massless Nambu-Goldstone bosons are expected, which corresponds to the α -type magnon. The symmetry breaking by the FM order is the same. In this case, the α -type magnon is the Nambu-Goldstone bosons.

F Additional figures

The dispersion relations for α - and β -type magnons under the FM order are shown in Figs. 11 and 12, respectively.

As the AFM order, we expect a gapless mode under the FM in the case of $d_1 = d_2 = 0$. In fact, we found the α -type magnon becomes gapless at $\mathbf{k} = \mathbf{0}$. While it is gapless, the mode turns out to be unstable. Here ‘unstable’ means

$$\tilde{\Gamma}_F^\alpha(0, \mathbf{k}) < 0, \quad (\text{F.1})$$

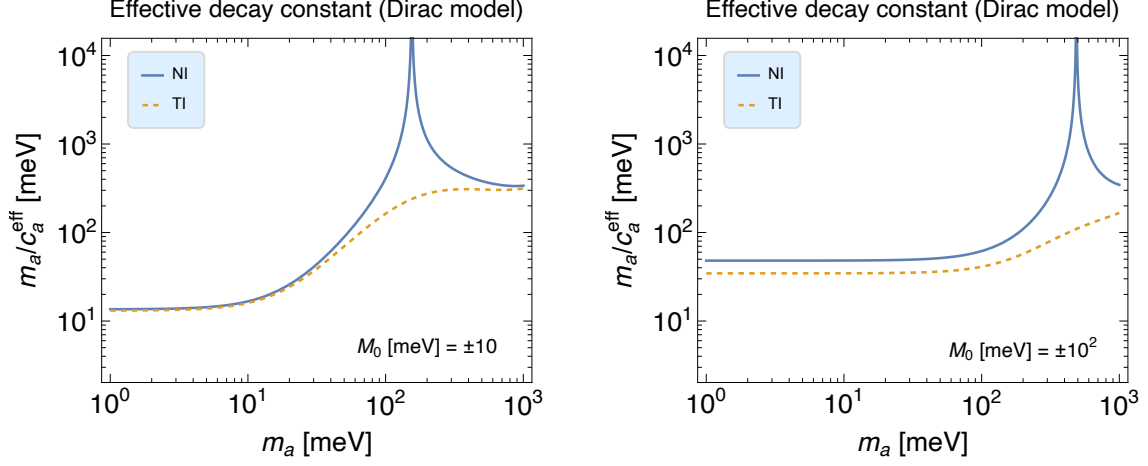


Figure 13. Same as Fig. 9 computed in the Dirac model. M_0 [meV] = ± 10 (left) and $\pm 10^2$ (right) are taken, where positive (negative) M_0 corresponds to the NI (TI) phases. The other parameters are taken as $A_1 = A_2 = 1$ eV.

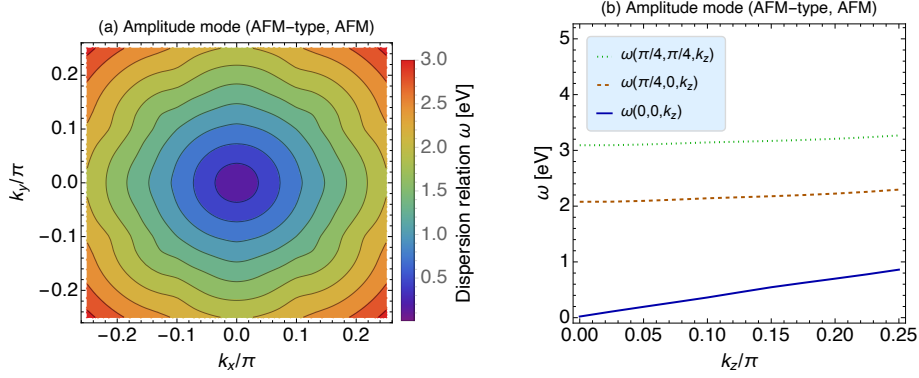


Figure 14. Same as Fig. 5 but using another values for A_1, A_2, B_1, B_2, M_0 that are given by Ref. [13].

around $\mathbf{k} = 0$. Namely, the spatial kinetic term has the opposite sign. Thus, such a mode is regarded as unphysical.

Fig. 13 shows the effective decay constant computed in the Dirac model. The Dirac model is given by expanding d_a in Eq. (3.8) around $\mathbf{k} = 0$. Using the same coefficients in the 3D TI model, we parametrize the Dirac model as

$$(d_1, d_2, d_3, d_4) = (A_2 k_x, A_2 k_y, A_1 k_z, M_0). \quad (\text{F.2})$$

Finally, the dispersion relation of the AFM-type amplitude mode by using the parameters given in Ref. [13] is given in Fig. 14. As in Fig. 5, the stability of this excitation is confirmed. In regions where $|k_x|$ and $|k_y|$ are large, the contours behave differently, but this is due to the relatively large value of $|B_2|$, which is affected by the boundary in the

wavenumber space integration. The behavior around $\mathbf{k} \sim 0$ is close to linear dispersion, which is simply because the gap is much smaller than eV.

References

- [1] J. Preskill, M. B. Wise, and F. Wilczek, Phys. Lett. B **120**, 127 (1983).
- [2] L. F. Abbott and P. Sikivie, Phys. Lett. B **120**, 133 (1983).
- [3] M. Dine and W. Fischler, Phys. Lett. B **120**, 137 (1983).
- [4] D. J. E. Marsh, K.-C. Fong, E. W. Lentz, L. Smejkal, and M. N. Ali, Phys. Rev. Lett. **123**, 121601 (2019), arXiv:1807.08810.
- [5] Y. Tokura, K. Yasuda, and A. Tsukazaki, Nature Reviews Physics **1**, 126 (2019).
- [6] B. A. Bernevig, C. Felser, and H. Beidenkopf, Nature **603**, 41 (2022).
- [7] J. Liu and T. Hesjedal, Advanced Materials **35**, 2102427 (2023).
- [8] A. Sekine and K. Nomura, Journal of Applied Physics **129** (2021).
- [9] R. Li, J. Wang, X. Qi, and S.-C. Zhang, Nature Phys. **6**, 284 (2010), arXiv:0908.1537.
- [10] K. Ishiwata, Phys. Rev. D **104**, 016004 (2021), arXiv:2103.02848.
- [11] K. Ishiwata, Phys. Rev. B **106**, 195157 (2022), arXiv:2206.00841.
- [12] L. Cao *et al.*, Phys. Rev. B **104**, 054421 (2021).
- [13] Y. Li *et al.*, Phys. Rev. B **102**, 121107 (2020), arXiv:2001.06133.
- [14] J. Wang, B. Lian, and S.-C. Zhang, Physical Review Letters **115** (2015).
- [15] M. N. Y. Lhachemi and I. Garate, Phys. Rev. B **109**, 144304 (2024), arXiv:2311.10674.
- [16] B. Lake, D. A. Tennant, and S. E. Nagler, Phys. Rev. Lett. **85**, 832 (2000).
- [17] A. Zheludev, K. Kakurai, T. Masuda, K. Uchinokura, and K. Nakajima, Phys. Rev. Lett. **89**, 197205 (2002).
- [18] C. Rüegg *et al.*, Phys. Rev. Lett. **93**, 257201 (2004).
- [19] C. Rüegg *et al.*, Phys. Rev. Lett. **100**, 205701 (2008).
- [20] A. Jain *et al.*, Nature Physics **13**, 633–637 (2017).
- [21] T. Hong *et al.*, Nature Physics **13**, 638–642 (2017).
- [22] S. Hayashida *et al.*, Phys. Rev. B **97**, 140405 (2018).
- [23] S. Hayashida *et al.*, Science Advances **5** (2019).
- [24] C. Herring and C. Kittel, Phys. Rev. **81**, 869 (1951).
- [25] C. Herring, Phys. Rev. **85**, 1003 (1952).
- [26] C. Herring, Phys. Rev. **87**, 60 (1952).
- [27] J. König, T. Jungwirth, and A. H. MacDonald, Phys. Rev. B **64**, 184423 (2001).
- [28] Y. Araki and K. Nomura, Phys. Rev. B **93**, 094438 (2016).
- [29] H. Zhang *et al.*, Nature Phys. **5**, 438 (2009).
- [30] C.-X. Liu *et al.*, Physical Review B **82** (2010).

- [31] G. Rosenberg and M. Franz, Physical Review B **85** (2012).
- [32] D. Kurebayashi and K. Nomura, Journal of the Physical Society of Japan **83**, 063709 (2014).
- [33] J. Wang, B. Lian, and S.-C. Zhang, Phys. Rev. B **93**, 045115 (2016), arXiv:1512.00534.
- [34] A. Sekine and K. Nomura, Phys. Rev. Lett. **116**, 096401 (2016), arXiv:1508.04590.
- [35] J. Schütte-Engel *et al.*, JCAP **08**, 066 (2021), arXiv:2102.05366.
- [36] H. Ooguri and M. Oshikawa, Phys. Rev. Lett. **108**, 161803 (2012), arXiv:1112.1414.
- [37] J. Zhang *et al.*, Chinese Physics Letters **37**, 077304 (2020).
- [38] S. Chigusa, T. Moroi, and K. Nakayama, JHEP **08**, 074 (2021), arXiv:2102.06179.